SOME ELECTRONIC PROPERTIES

OF ZnO AND SrTiO$_3$

Thesis by

Richard C. Neville

In Partial Fulfillment of the Requirements

For the Degree of

Doctor of Philosophy

California Institute of Technology

Pasadena, California

1971

(Submitted May 19, 1971)

ACKNOWLEDGEMENTS

iii

ABSTRACT

The surface barrier systems consisting of gold and palladium on both chemically prepared and cleaved zinc oxide have been studied in detail. Surface barrier energies on non-degenerate chemically prepared zinc oxide were found to be 0.66 and 0.60 eV respectively for gold and palladium, as determined by four independent methods: photoresponse, current-voltage characteristics, thermal activation energy, and capacitance variation with voltage. The Bethe diode theory as modified by image force lowering was found to be an excellent description of the voltage-current characteristics. Thermionic field and pure tunneling currents were observed for surface barriers on degenerate zinc oxide at room and liquid nitrogen temperatures, respectively. The voltage dependence of these currents was in excellent agreement with the thermionic field and tunneling theories. Although dependence on impurity concentration was functionally in agreement with theory the predicted currents were too high by an order of magnitude. This effect is attributed to deficiencies in the theory.

The second material investigated was strontium titanate. The surface barrier systems consisting of gold, palladium, copper, and indium on both chemically prepared and cleaved single crystal strontium titanate were examined in detail. Surface barrier energies were determined, and the current versus voltage characteristics were examined in light of Bethe diode theory as modified by image force lowering. The relative permittivity of strontium titanate was determined over a temperature range from 4.2°K to 300°K as a function of applied electrical bias. No evidence of a ferroelectric transition was observed. A phenomonological description

of the free energy involved in the titanium atom motion, which is responsible for the large relative permittivity, was derived. Evidence for domain interaction is discussed.

TABLE OF CONTENTS

Chapter 1

ZINC OXIDE

1.1 Introduction

As a material, the hexagonal crystal, II-VI compound zinc oxide has
been known since the archaeological Bronze Age and has been put to uses
ranging from ladies' face powder to photocopying processes[1]. Investi-
gations into the electronic properties of this hexagonal crystal have
been undertaken only relatively recently. The energy band gap has been
found to be 3.435 eV[2] and the material, when pure, acts as an insula-
tor[1]. Reduction of the crystal yields oxygen vacancies which act as
donors[1]. In 1958 and 1961 Rupprecht[3] and Bogner[4] determined the
carrier mobility of non-stoichiometric bulk samples of zinc oxide. The
dielectric constant for zinc oxide was determined by Collins and
Kleinman[5] in 1958. In 1961 Dietz et al.[6] measured the effective mass
of the conduction band electrons in this material. In 1965 Mead[7]
determined the surface barrier energies of several metals on vacuum-
cleaved zinc oxide. In spite of much investigation, two areas of basic
importance are as yet untouched. To obtain full understanding of the
surface barrier properties of this typical, two element, ionic semicon-
ductor[7,8] it was necessary to measure and analyze the surface barrier
energies and current-voltage characteristics of Schottky barriers on
chemically prepared, non-degenerate, zinc oxide surfaces. Secondly,
with this understanding of the non-degenerate material, it is then
possible to use degenerate zinc oxide to study currents arising from
quantum mechanical tunneling through the surface barrier and to test

the validity of the theories concerning tunneling currents.

A complete examination into the Schottky barrier properties of non-degenerate zinc oxide was conducted. At the same time bulk measurements of resistivity and mobility were made. These studies were conducted on samples varying from approximately 10^{16} to 10^{18} per cubic centimeter in carrier concentration. An extensive investigation of the metal-semiconductor barrier systems formed by gold and palladium on zinc oxide was carried out, by four independent methods: photoresponse, forward current-voltage characteristics, thermal activation energy and capacitance variation with voltage. Also forward and reverse current-voltage characteristics on non-degenerate material were studied and analyzed in terms of simple Bethe thermionic diode theory[9] as modified by image force lowering. Additional measurements of reverse biased current and capacitance yielded energy level and concentrations of the traps in the crystal. A unique understanding of the surface barrier properties of an ionic semiconductor was gained.

In highly doped degenerate, n-type, semiconductors the Fermi level lies in the conduction band. At sufficiently low temperatures, Schottky barrier current conduction is through the surface barrier by pure field emission (tunneling). As the temperature is raised electrons are thermally excited to energies which are a significant fraction of the barrier energy. At these energies the electrons tunnel through an energy barrier much thinner than the surface barrier thickness at the Fermi level. This current mode, combining thermionic and tunneling mechanism, is known as thermionic-field emission or TFE. First order theoretical aspects of TFE and tunneling current conduction for Schottky barriers on various

degenerate semiconductors have been treated by Padovani and Stratton[10], Conley and Mahan[11], Millea et al.[12], Parker and Mead[13], and Parker[14] among others. They found that the effective mass of the charged particles which make up the current is of major importance in tunneling and TFE theories[10,12]. Investigations have been conducted with materials of effective electron mass less than one-tenth the free electron mass[12,14] yielding results within a factor of two of theory. Zinc oxide has an effective electron conduction band mass of 0.38 the free electron mass[6]. Examination of the current voltage characteristics of Schottky barriers on zinc oxide affords an examination of the theories for tunneling and TFE currents as extrapolated to high mass materials.

An examination of the current-voltage characteristics of gold and palladium surface barriers was conducted on degenerate zinc oxide. The temperature was varied to afford an opportunity to study both tunneling and TFE currents. Surface barrier energies were determined by photo-response and compared to the measurements on non-degenerate material. Measurements of individual barrier capacitance served as a confirmation of carrier concentration as determined from Hall and resistivity measurements ($\sim 10^{18}$-10^{20}/cm^3) and provided a localized carrier concentration useful for the theoretical calculations. This study of tunneling and thermionic currents clearly indicates the need for some change in the theory, since, as will be shown, predicted tunneling currents are an order of magnitude different from the actual current.

1.2 Description and Preparation of the Material

Several zinc oxide crystals of two types were used in these

4

experiments. Four, undoped, clear hexagonal zinc oxide crystals with a free electron concentration, resulting from non-stoichiometry[1], of between 1×10^{16} and 2×10^{17} per centimeter cubed were used in the initial investigation of surface barrier energy on chemically prepared surfaces. Three indium doped degenerate hexagonal crystals of zinc oxide were used in studies of degenerate material. The typical crystal was 2 cm in length with each of the six lateral faces being 0.2 cm in width.

All crystals were initially cleaned by etching in concentrated phosphoric acid for 15 minutes, followed by a 10 minute soak in concentrated hydrochloric acid to remove phosphates. The crystals were then rinsed in flowing deionized water and dried in a jet of dry filtered air. Five contacts were soldered onto each crystal bar (see Fig. 1.1 for a typical contact configuration) and Hall and resistivity measurements were made. The solder used was a low temperature melting 90% indium-10% silver solder. After resistivity and Hall measurements were made the solder was removed in hydrochloric acid, the samples rinsed with water and dried with a jet of dry, filtered air. The samples were then stored until surface barriers were placed on them.

To produce a surface barrier the crystal samples were first cleaned as above. The samples were next placed in a ion-pumped vacuum chamber at a pressure nominally less than 10^{-6} Torr. Using a heated tungsten filament approximately ~1,000 Å of gold or palladium was evaporated on the lateral surfaces of the sample through a fine mesh screen. Nominal surface barrier contact diameter was 100 microns. Contact to the evaporated barriers was made by a fine gold-wire probe
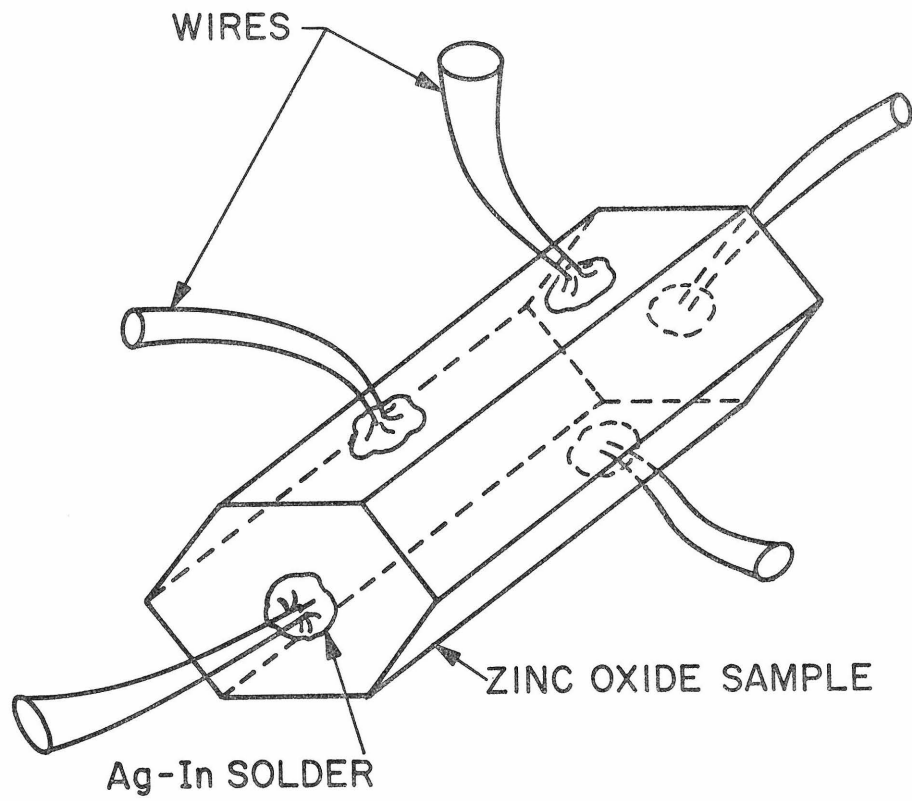
WIRES

ZINC OXIDE SAMPLE

Ag-In SOLDER

Fig. 1.1 Contact configuration for Hall and resistivity measurements.

in a three dimensional micro-manipulator. Bulk contacts were soldered onto each crystal using a 90% indium-10% silver solder. A three point differential measurement was used to eliminate excessive voltage drops from the non-ideal nature of the bulk crystal contacts. By repeating the surface cleaning and barrier formation processes both gold and palladium barriers were formed on each sample.

After measurement of the barriers on the lateral surfaces some of the zinc oxide crystals were cleaved, in air, along the basel plane. These crystals were placed in an ion-pumped vacuum at less than 10^{-6} Torr within two minutes of cleaving. Surface barriers were next evaporated on the basel plane, contacts soldered to the bulk and electrical measurements performed as in the case of the chemically prepared surfaces.

1.3 Bulk Measurements

Resistivity and mobility measurements were made on the zinc oxide crystals at both room temperature (296°K) and at liquid nitrogen (77°K) temperature. The resistivity measurement was a simple four point measurement using the two end contacts in Fig. 1.1 to supply current and the two top contacts to measure potential drop. The Hall measurement used for determining mobility was made using a 4.7 kilo Gauss permanent magnet and the Hall voltage was determined from two contacts on opposite sides of the crystal (Fig. 1.1). Care was exercised to assure that only the Hall voltage was measured at the Hall contacts. The resistivity was then combined with the mobility data to derive an effective donor concentration of:

$$N_d = \frac{1}{\rho\mu q} \hspace{6cm} (1.1)$$

Where: N_d is the ionized donor concentration

   ρ is the measured resistivity

   μ is the conductivity mobility[15,16]

   q is the electronic charge

Typical measured values of resistivity and mobility and the resultant effective carrier concentration are presented in Table 1.1. The mobility values are typical of those reported in the literature[3,4].

1.4 Surface Barrier Energy Measurements on Non-Degenerate Material

When a metal and semiconductor are placed in intimate contact the vacuum energy level for electrons remains fixed. The work functions of the two materials are not identical. Combined with the requirement that the Fermi levels in equilibrium are in alignment the result is an energy variation with distance given in Fig. 1.2a. The surface barrier energy, ϕ, is the difference between the Fermi level and the conduction band edge at the metal semiconductor interface. The Fermi level for non-degenerate semiconductors lies below the conduction band edge in the bulk material. The shape of the conduction band edge near the surface barrier is parabolic[9]. The distance into the semiconductor at which the conduction band edge becomes fixed, relative to the Fermi level, is dependent inversely on the impurity concentration. Electrons in the metal are thermally excited to energies greater than ϕ. One-half of these then travel across the barrier from left to right. Thermally excited electrons from the semiconductor travel in the opposed direction

Sample Crystal No.	1	2	3	4	5	6	8
Resistivity at 290°K (Ω-cm)	1.04	1.51	1.80	.17	5.6×10^{-3}	3.2×10^{-3}	4.0×10^{-3}
Resistivity at 77°K (Ω-cm)	1.98	2.20	3.10	.25	5.8×10^{-3}	3.3×10^{-3}	4.3×10^{-3}
Mobility at 296°K (cm^2/V sec)	200	176	200	190	49	58	55
Mobility at 77°K (cm^2/V sec)	300	260	300	220	43	56	49
Carrier Concentration at 296°K (cm^{-3})	3×10^{16}	2.36×10^{16}	1.75×10^{16}	1.93×10^{17}	2.3×10^{19}	3.5×10^{19}	2.85×10^{19}
Carrier Concentration at 77°K (cm^{-3})	1.05×10^{16}	1.1×10^{16}	$.67 \times 10^{16}$	1.14×10^{17}	2.5×10^{19}	3.4×10^{19}	3×10^{19}

TABLE 1.1

Resistivity, Mobility, and Carrier Concentration of Typical Zinc Oxide Specimens
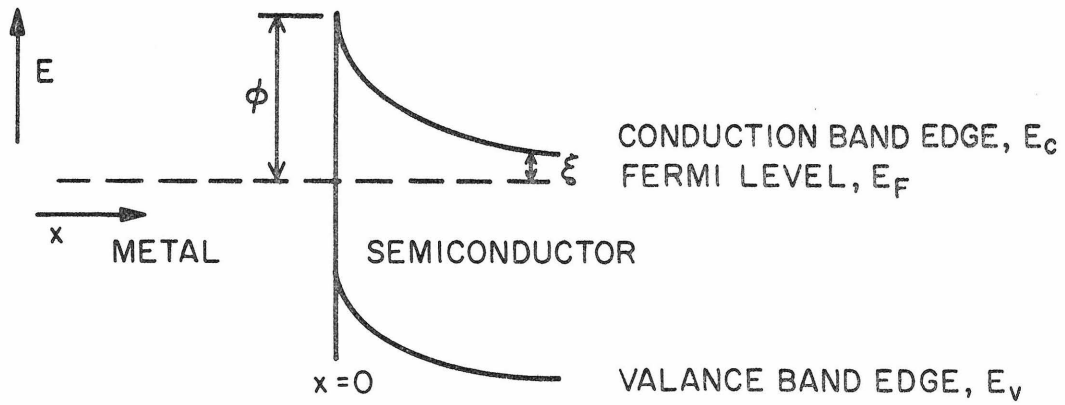
Fig. 1.2a Metal – semiconductor barrier electron energy and
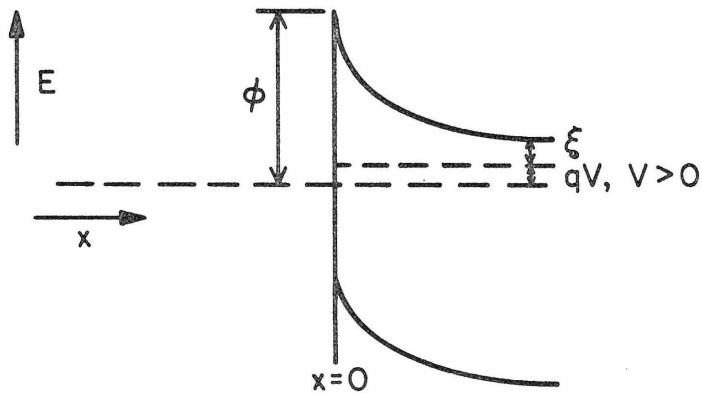distance relationships under equilibrium conditions.

Fig. 1.2b Metal – semiconductor barrier electron energy and
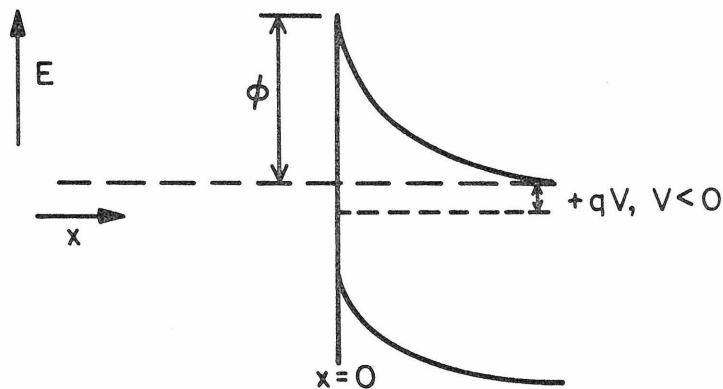distance relationships under forward bias.

Fig. 1.2c Metal – semiconductor barrier electron energy and
distance relationships under reverse bias.

creating a zero equilibrium current.

Application of a positive voltage (forward bias) to the metal results in the energy band picture of Fig. 1.2b. I have suppressed small potential changes owing to current flow in order to simplify the picture. Under these conditions large numbers of electrons in the conduction band are thermally excited to levels above the surface barrier and cross into the metal. Bethe[9] has treated this condition in detail. The pertinent equations are given in Appendix A.

Application of negative voltage (reverse bias) to the Schottky barrier produces the energy changes shown in Fig. 1.2c. It is now less probable that electrons in the semiconductor will thermally acquire an energy in excess of the barrier energy. The thermally generated electron current from the metal is dominant[9].

Surface barrier energies on non-degenerate zinc oxide were determined by using four independent techniques: photoresponse, forward current-voltage characteristics, thermal activation energy, and capacitance variation with applied voltage. In photoresponse a shorted barrier is exposed to light of varying energy. The photons excite electrons and current is observed for photon energies in excess of the barrier energy. Forward current-voltage techniques make use of electrical energy to alter the equilibrium energy balance and produce an excess of current in one direction. The current is dependent on the applied voltage and barrier energy. Thermal activation energy techniques vary the temperature while the barrier is reverse biased. The non-equilibrium current is a function of the thermal energy of the electrons and of the barrier energy. Lastly, capacitance voltage techniques use

the dependence of the capacitance upon the voltage and barrier energy to obtain the barrier energy (Appendix B).

1.4.1 Photoresponse

The barrier energy was determined by a measurement of the photo-current in a shorted diode. A tungsten-halide lamp was used as the light source for a Gaertner quartz prism monochronometer. The light was chopped at 50 Hz and a lock-in amplifier was used to improve the signal-to-noise ratio. The photons must be absorbed near the surface barrier in order to generate carriers which will cross the barrier before undergoing collisions with the lattice. The crystal samples, being approximately .3 cm thick, were too thick to get a sufficient photon flux at the barrier. Therefore, the barrier side was exposed to the photon flux. This made it necessary to keep the surface barrier metal thickness to a 1500 $\overset{\circ}{A}$ maximum.

In Fig. 1.3 the photoresponse, the square root of the short circuit barrier currents, per incident photon, is presented for typical surface barriers. The expected[17] straight line response is followed except at high photon energies. There surface scattering and absorption effects reduce the number of photons reaching the barrier.

1.4.2 Forward Current Versus Voltage

The sample barriers were measured using a five place digital volt-meter and an operational amplifier type current meter capable of measuring currents from 1 pA to 10 mA. The current source for the diode was a battery with an adjustable resistor. Individual barrier area was approximately 8×10^{-5} cm^2. Measurements were made with a three contact configuration (Fig. 1.4) to eliminate excessive potential drop at the bulk
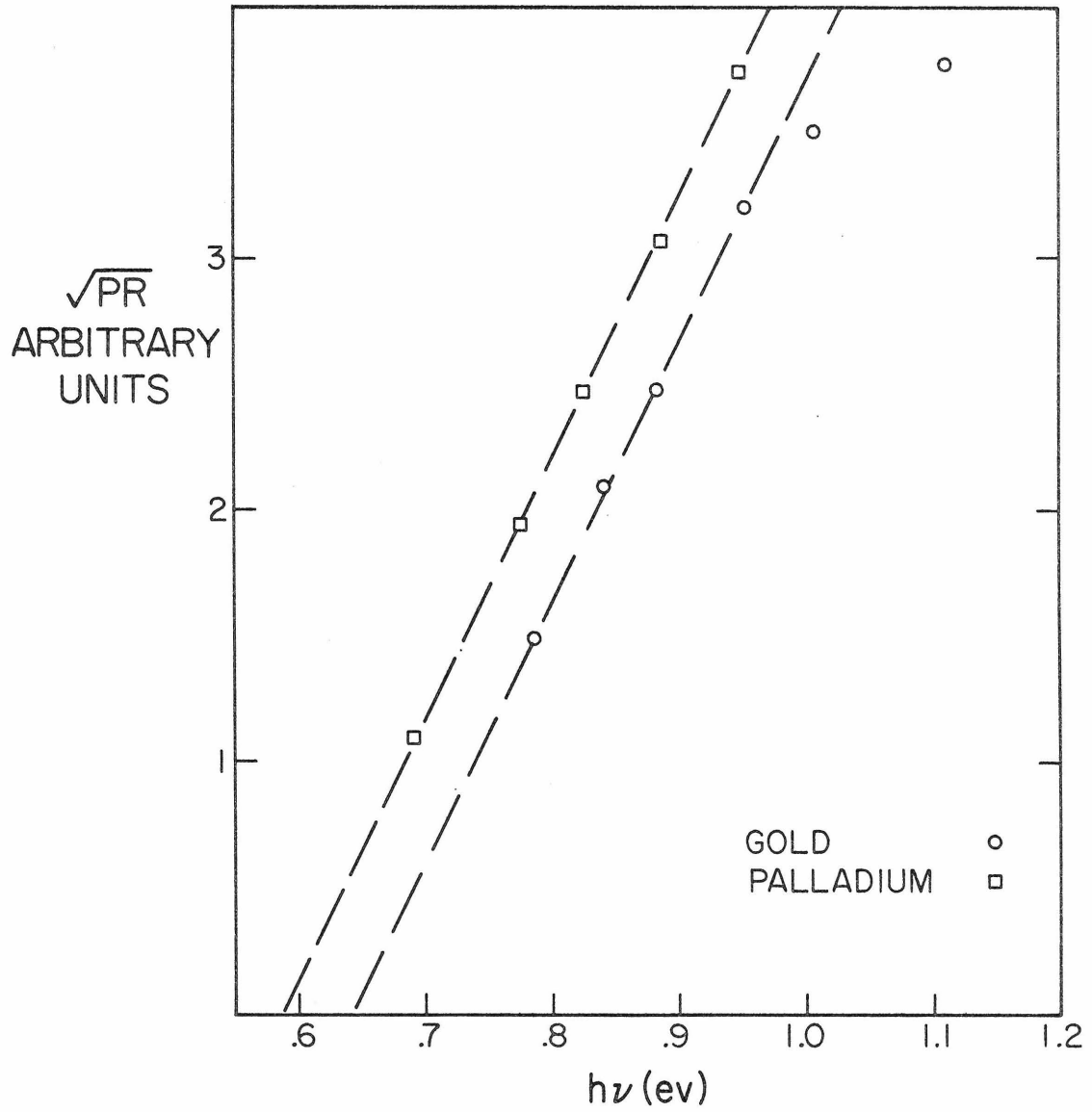
Fig. 1.3 Square root of photocurrent per incident photon versus photon energy for typical gold and palladium surface barriers on zinc oxide at 300°K.
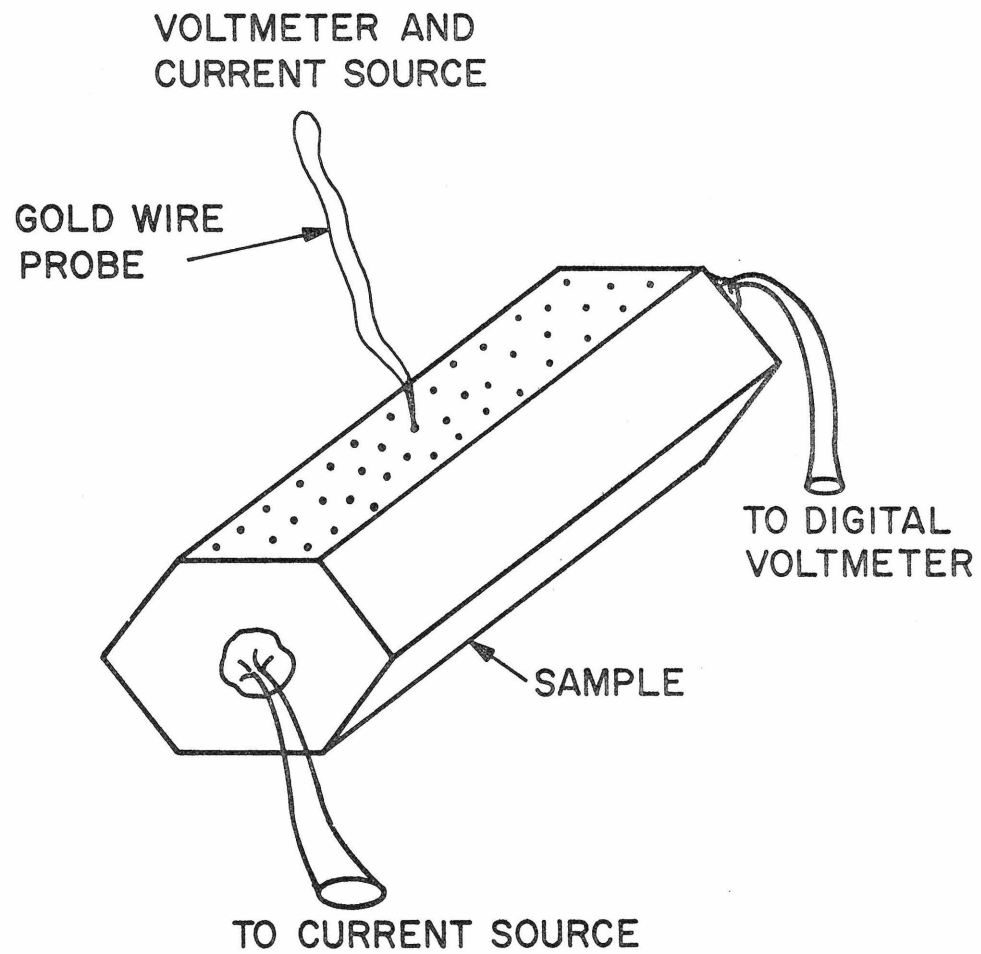
Fig. 1.4 Typical current test configuration with three leads.

crystal contact. The measurements were conducted with no illumination to avoid generation-recombination current.

Typical curves of the logarithm of the forward current density versus forward voltage are presented in Fig. 1.5 for gold and palladium on chemically cleaned zinc oxide. The region of linear behavior of the log current versus voltage is in excess of two orders of magnitude. This linear region is limited by series resistance effects at large currents and by reverse current at small voltages. The slope of the curves is approximately 60 mV per decade of current. Typical values of the extrapolated zero voltage current intercept are 7×10^{-3} A/cm^2 for palladium surface barriers and 8×10^{-4} A/cm^2 for gold barriers on zinc oxide.

1.4.3 Thermal Activation Energy

A third determination of the surface barrier energy was obtained from the measurement of reverse current as a function of temperature while maintaining a fixed reverse bias. The temperature was varied by using a Peltier cooler-heater. The barriers were biased with a battery powered, temperature stable, transistorized power supply. Current was measured with a picoammeter. All measurements were made with no illumination to avoid generation-recombination currents.

In Fig. 1.6 the logarithm of the reverse current versus the inverse temperature for typical gold and palladium surface barriers is presented. The behavior is a straight line consistent with exponential behavior.

1.4.4 Capacitance Measurements

The final determination of surface barrier energies on zinc oxide was made using the variation of barrier capacitance with applied voltage. The measurements were made in total darkness to eliminate effects from
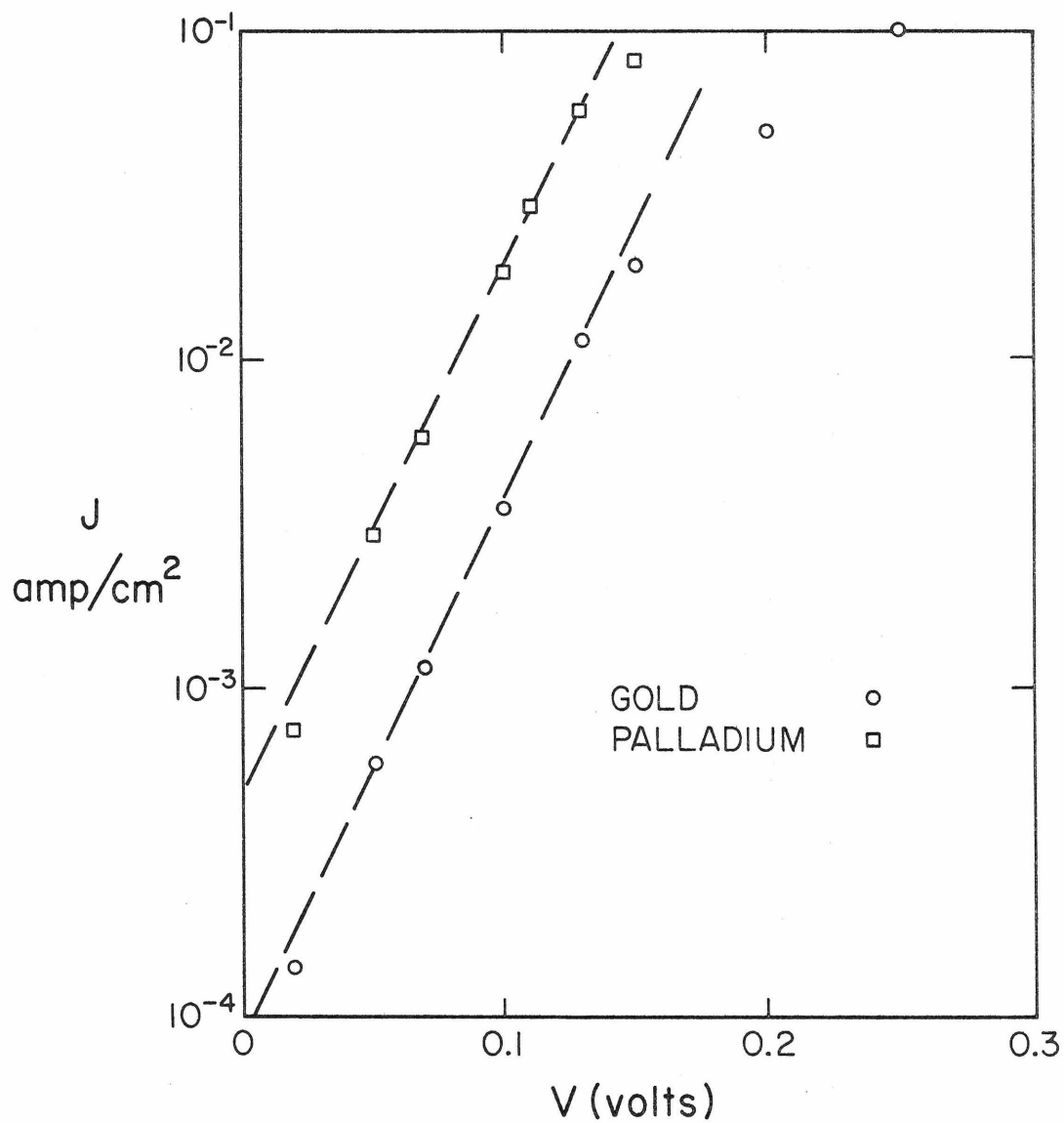
Fig. 1.5 The logarithm of the forward current density as a function of forward voltage for typical gold and palladium surface barriers on zinc oxide at 300°K.
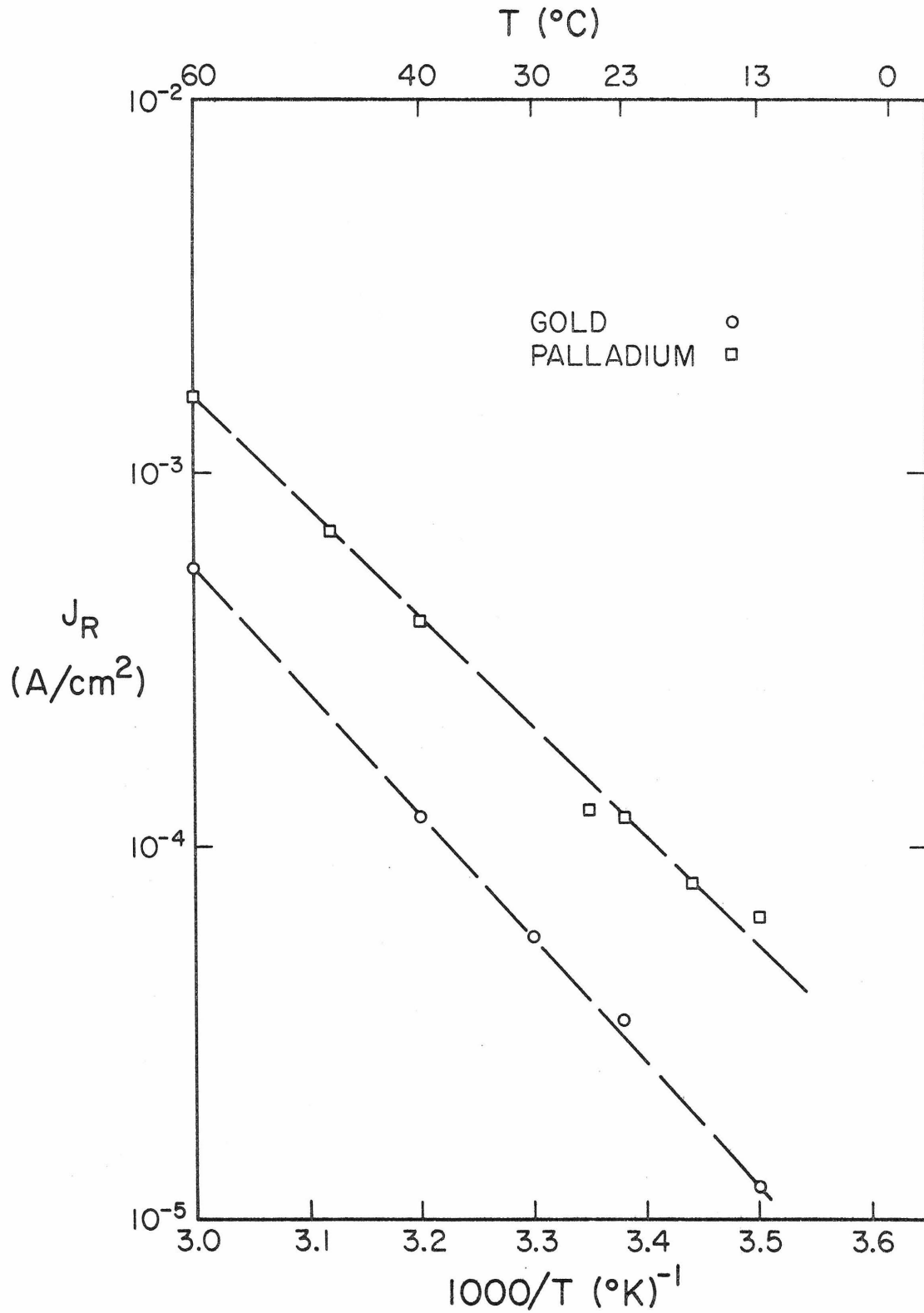
Fig. 1.6 Log current density as a function of inverse temperature for gold and palladium barriers on nondegenerate zinc oxide at a reverse bias of 1 volt.

charged trap sites. A capacitance bridge and a L-C meter were used, both at a frequency of 1 MHz. Variable bias was supplied by the bridge and through the L-C meter. Stray capacitance in the leads was determined and eliminated. Measurements under forward bias conditions were not made because of the large currents involved.

In Fig. 1.7 there are presented values of the inverse capacitance squared versus voltage for gold and palladium surface barriers under both non-illuminated conditions and illumination with 0.5 micron light. The observed behavior of $1/C^2$ versus V was in a straight line for bias levels to -10 volts. Fig. 1.7 shows only a portion of the data in order to allow examination of the infinite capacitance intercept. The illuminated measurements were to investigate bulk trapping sites and will be discussed in Section 1.5.

1.4.5 Barrier Energy Summary and Discussion

The values of the surface barrier energy for gold and palladium on chemically prepared zinc oxide were obtained from photoresponse, current-voltage characteristics, thermal activation energy and capacitance variation with voltage techniques. These values are presented in Table 1.2. Also given are overall averages for the surface barrier energies.

The surface barrier energies for photoresponse were found from the photon energy for the extrapolated square root of the short circuit photo current at zero current in Fig. 1.3, in accord with simple Fowler theory (see Appendix A for a synopsis of the theory).

The current-voltage characteristics of gold and palladium surface barriers were presented in Fig. 1.5. From the Bethe[9] theory for thermionic diodes as modified by image force lowering it is possible to
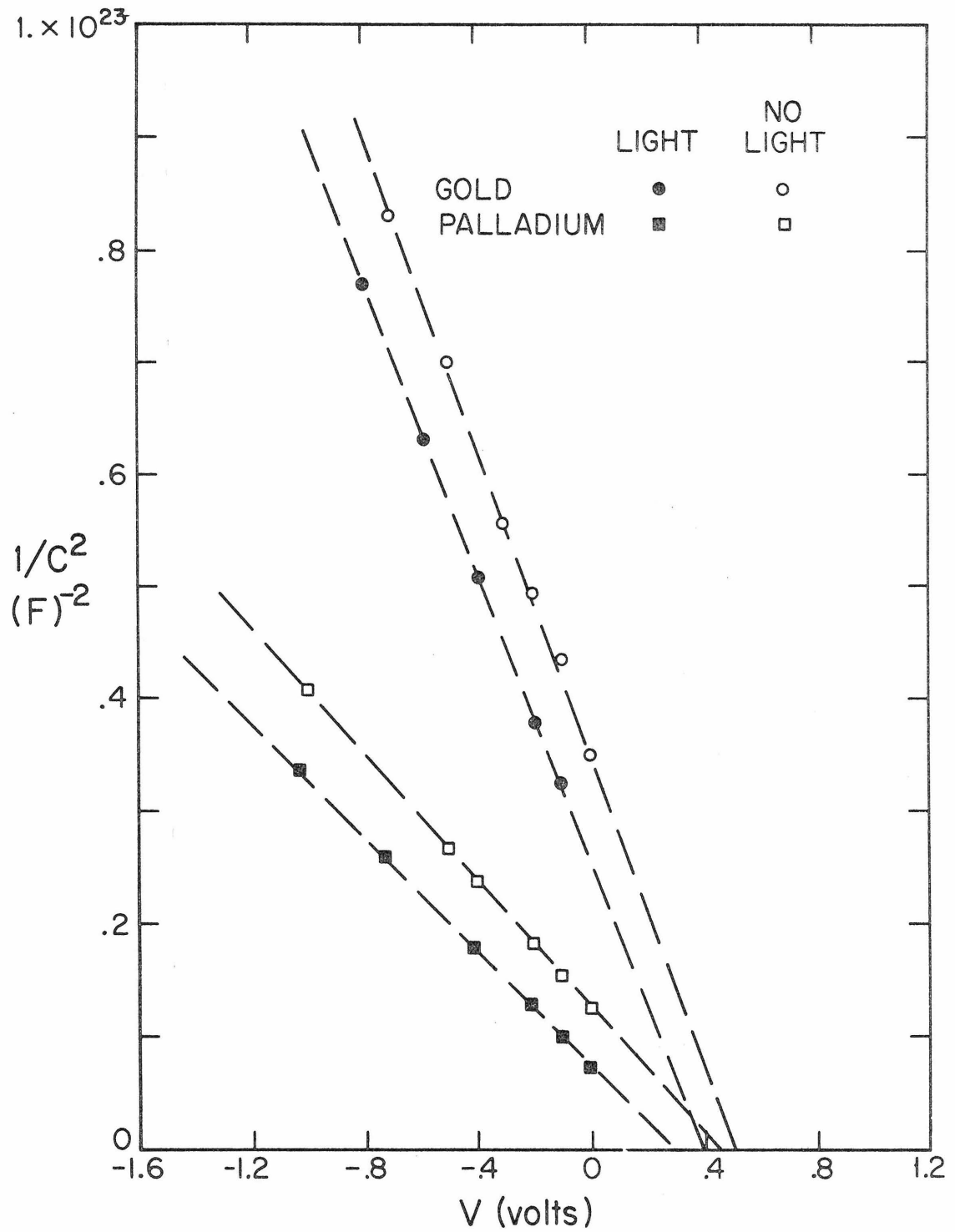
Fig. 1.7 Inverse capacitance squared as a function of bias for gold and palladium barriers on zinc oxide at room temperature. Measurement frequency was 1 MHz.

Metal	Gold	Palladium
	Barrier Energy (electron volts)	
Photoresponse	0.645 ± 0.04	0.59 ± 0.04
I-V Characteristics	0.66 ± 0.03	0.60 ± 0.04
Activation Energy	0.65 ± 0.04	0.59 ± 0.04
Capacitance - Voltage	0.67 ± 0.03	0.61 ± 0.05
Average	0.66 ± 0.04	0.60 ± 0.04

TABLE   1.2

Surface Barriers Energies

on

Chemically Prepared

Zinc Oxide

determine the surface barrier energies from a knowledge of the slope and
the extrapolated zero bias current intercept (see Appendix A). For ap-
plied forward bias well in excess of kT/q the theory predicts that the
log current versus voltage characteristics will be a straight line, as
was observed. Here k is the Boltzman constant and T the temperature.

The ideal log current-voltage slope from the Bethe diode theory is
59.8 mV per decade of current. Image force lowering modifies this by a
multiplicative factor of n, known as the diode non-ideality factor.
Experimentally, the value of n was found to be 1.05 ± 0.05. Appendix A
contains a computation of n. Using an optical frequency dielectric
constant of 4[21] and a low frequency dielectric constant of 8[5], the
predicted value of n is 1.05. This confirms that image force lowering
is present. The surface barrier energies presented in Table 1.2 were
determined using the observed value of n and extrapolated zero current.

The reverse current of a surface barrier is dependent on the surface
barrier energy. The surface barrier energy is a function of temperature.
In Appendix A the effects of barrier temperature variation on the observed
temperature variation of the reverse current are considered. The reverse
current data presented in Fig. 1.6 were used to calculate surface barrier
energies accounting for the barrier temperature variation effect.

The surface barrier energy can be obtained from capacitance measure-
ments by observing the infinite capacitance intercept. This intercept is
related to the barrier energy by the Fermi level (Appendix A). The Fermi
level is a function of the impurity concentration (Appendix B). The
impurity concentration can be derived from the slope of the $1/C^2$ versus
V curve of Fig. 1.7. Using the non-illuminated data, carrier concentrations

were determined for the individual barriers. The average values are in good agreement with Hall and resistivity derived carrier concentrations and are presented in Table 1.3. The individual surface barrier carrier concentrations were then used to determine surface barrier concentrations from the intercepts.

In summary, the surface barrier energies measured by all four methods are in excellent agreement. The current-voltage characteristics are clearly due to thermionic currents as modified by image force lowering. The variation of barrier energy with temperature correction, yields thermal activation surface barrier energies in agreement with the other methods. No effects of carrier concentration on surface barrier energy were observed. The overall picture is of a material with a "textbook" behavior, a very rare occurrence.

1.5 Other Measurements

Besides the surface barrier energy measurements on chemically prepared surfaces a number of additional measurements were made both to investigate other properties of this material and to link this particular material to previous measurements[7].

1.5.1 Cleaved Barriers

Gold and palladium surface barrier energies on cleaved zinc oxide were measured by photoresponse and capacitance versus voltage techniques. The values obtained were found to be identical with those in the literature[7]. The work in the literature[7] dealt with vacuum cleaved samples while the work reported on here was with chemically prepared samples. Clearly, exposure to air for two minutes has a minimal effect on

Sample	1	2	3	4
N_d(Hall-Resistivity) cm^{-3}	3×10^{16}	2×10^{16}	1.75×10^{16}	1.65×10^{17}
N_d(C-V slope) cm^{-3}	3.1×10^{16}	2×10^{16}	1.9×10^{16}	1.8×10^{17}

TABLE 1.3

Carrier Concentration as Determined by Hall-Resistivity and
Capacitance-Voltage Techniques on Non-Degenerate Zinc Oxide

the surface states and therefore, observed surface energies[7].

1.5.2   Reverse Current and Voltage Methods

The voltage dependence of the reverse current characteristic, at a fixed temperature, as a function of the fourth root of the applied voltage is shown as a straight line in Fig. 1.8, where V_o is the barrier energy less Fermi level and kT/q.   The bias voltage was applied using a battery and variable resistor.   Currents were measured using a picoammeter. The measurements were made in the dark to eliminate generation recombination currents.   The ideal reverse current, independent of the applied reverse voltage, of the Bethe diode theory is modified by the presence of the image force field lowering.   This results in a barrier energy change with applied voltage[19].   The theoretical slope of the logarithm of the reverse current versus voltage can be found in Appendix A Eqs. (A.19, A.22).   The theoretical results are plotted in Fig. 1.8.   The experimental and theoretical agreement is excellent over a wide range in applied voltage in both voltage dependence and in magnitude.   This is additional confirmation that zinc oxide is an ideal material in its barrier properties.   The reverse current of the surface barriers was next measured as a function of wavelength of the light shining on the sample.   The samples were illuminated by a mineral lamp with a number of filters of differing cutoff wavelength.   An increase in current was experienced for wavelengths in the 1.2-1.5 micron range.   From these data a trap energy level was estimated to lie between 0.8 and 1.0 electron volts.

The difference in carrier concentration determined from Fig. 1.7 under non-illumination and illumination is the result of photo excitation of carriers from trap sites into the conduction band leaving fixed charge
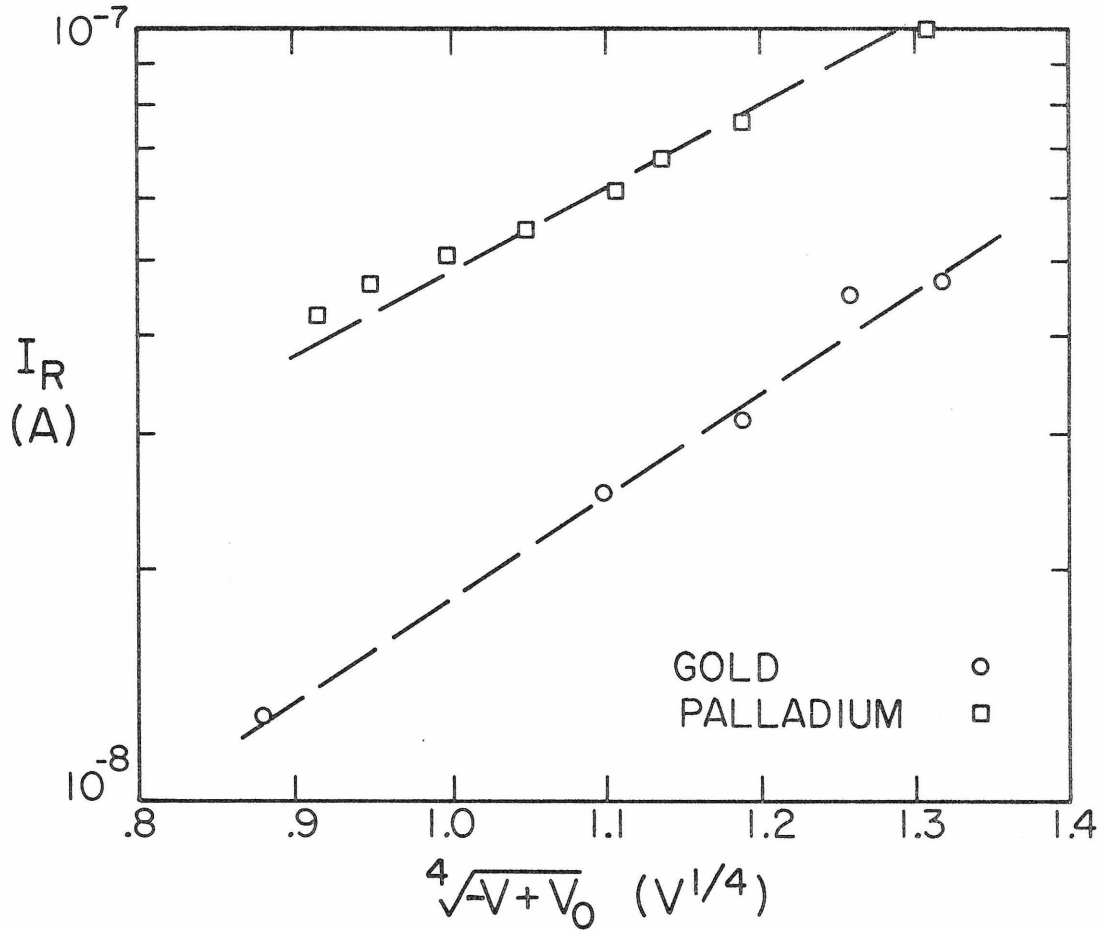
Fig. 1.8 Log reverse current versus the fourth root of voltage for
typical gold and palladium barriers on zinc oxide at room
temperature, where V_o is the barrier energy less Fermi
level and kT/q.

centers. The straight line data for illuminated inverse capacitance versus voltage indicate a uniform trap distribution. A lower bound for the trap density, N_T, can be estimated from:

$$N_T = N_d \text{ (illuminated)} - N_d \text{ (dark)} \qquad (1.2)$$

Values of N_d (illuminated), N_d (dark) and N_T are presented in Table 1.4. Minimum trap densities are approximately $\frac{1}{10}$ of the donor density and presumably arise from the same general source, the non-stoichiometry of the host crystal since they are proportional to the donor density.

1.6 Tunneling Studies with Degenerate Zinc Oxide

Pure tunneling current conduction is expected for surface barriers on degenerate zinc oxide at low temperatures. At room temperature surface barriers on degenerate zinc oxide should conduct current by a combination of pure tunneling and thermionic current modes known as thermionic field emission or TFE. This section is concerned with: 1) a study of the current modes exhibited by surface barriers on degenerate zinc oxide at 77°K and 300°K and 2) an investigation of the validity of the pertinent theories, summarized briefly in Appendix C, that describes these current modes. Such an investigation as this is possible because of the excellent understanding of surface barriers on zinc oxide gained in the previous sections.

The effective density of states, N_c, is equivalent to the number of electrons which can be in the conduction band with the Fermi level still in the forbidden gap. For n greater than N_c the material is degenerate

Metal	Illumination	Donor Concentration (cm^{-3})
Gold	Yes	3.3×10^{16}
	No	3.1×10^{16}
	Trap Density	$\geq 2 \times 10^{15}$
Palladium	Yes	2.2×10^{16}
	No	2.0×10^{16}
	Trap Density	$\geq 2 \times 10^{15}$
Palladium	Yes	2×10^{17}
Crystal 4	No	1.8×10^{17}
	Trap Density	$\geq 2 \times 10^{16}$

TABLE 1.4

Trap Concentration

and the Fermi level enters the conduction band. The conduction band
effective density of states, N_c, is given by[16]:

$$N_c = \frac{m^* kT}{2\pi\hbar^2}^{3/2} \qquad (1.2)$$

Where: m^* is the Boltzmann constant

T is the absolute temperature

$\hbar$ is Planck's constant divided by 2π.

The effective mass for ZnO is 0.38 times the free electron mass[6].
Therefore, the effective density of states is:

$$N_c(300°K) = 6 \times 10^{18}/cm^3$$
$$N_c(77°K) = 7.8 \times 10^{17}/cm^3 \qquad (1.3)$$

It can be seen from the Hall and resistivity derived carrier concentra-
tions, Sec. 1.3, that the indium doped samples 5, 6, 8 are degenerate
with the Fermi level well into the conduction band. At room temperature
the Fermi level lies between 0.03 and .120 eV above the conduction band
edge for carrier concentrations between 1×10^{19} and $5 \times 10^{19}/cm^3$. At
liquid nitrogen temperature the degeneracy lies between 0.047 and .143 eV
for the same range of concentrations. Therefore, crystals 5, 6, 8 are
ideally suited to study tunneling currents.

The theoretical calculations involved in a study of tunneling and
TFE currents depend upon a knowledge of the semiconductor impurity con-
centration associated with the surface barriers. This impurity concen-
tration can be determined from Hall and resistivity measurements on the
crystal, as a whole, a bulk average, or from capacitance measurements

for individual barriers. Capacitance variation with voltage, the method used to determine impurity concentration with non-degenerate zinc oxide, cannot be used because high tunneling currents make capacitance measurements at other than zero bias extremely difficult. The zero bias capacitance observed ranged from 100 to 200 pF and each was converted to a carrier concentration using Eq. (B.4). An average impurity concentration, as obtained from the unbiased capacitance, was calculated for each crystal sample by averaging the values found for barriers on all crystal surfaces. This value can be compared to the Hall-resistivity derived impurity concentration in Table 1.5. Agreement is poor indicating spatial fluctuations in the impurity concentration in the samples. Therefore, the individual surface barrier carrier concentration, as determined from capacitance measurements at zero bias, was used in the tunneling computations.

1.6.1 Measurements on Degenerate Material

Forward voltage-current characteristics were observed for gold and palladium surface barriers on both chemically prepared and on freshly cleaved zinc oxide surfaces. The measurements were made at both room and liquid nitrogen temperatures. The power supply consisted of a battery and a variable resistor. Current measurements between 10 pA and 10 mA were made with a sensitive picoammeter. Voltage was measured using a high imput impedance digital voltmeter. Capacitance measurements were made on each barrier using a bridge at a frequency of 1 MHz. All measurements were made under zero illumination conditions to eliminate generation-recombination current.

Sample	5	6	7
N_d(Hall-Resistivity) cm^{-3}	2.3×10^{19}	3.5×10^{19}	2.85×10^{19}
N_d(C(V=0)) cm^{-3}	2.5×10^{19}	5.1×10^{19}	1.7×10^{19}

TABLE   1.5

Carrier Concentration as Determined by Hall-Resistivity and
Capacitance-at-Zero-Voltage Techniques on Degenerate Zinc Oxide

Forward log current density is presented as a function of forward voltage for typical sample barriers at 77°K in Fig. 1.9 and at 300°K in Fig. 1.10. The current voltage characteristics are linear over a bias of several kT/q. At high current levels the series resistance of the contacts and of the bulk crystals reduces the current. At low levels reverse tunneling currents reduce the current level. However, in each surface barrier case, it can be seen that the linear region is sufficient to permit determination of the slope of the log current versus voltage curve and of the extrapolated zero bias current density.

1.6.2 Discussion of Tunneling Studies

The thermionic field emission (tunneling) theories are summarized in Appendix C. Each theory is applicable over a range of temperatures and impurity concentrations and those theoretical limits are expressed as Eq. (C.8), Eq. (C.13) and Eq. (C.14). For the individual impurity concentrations used here, the applicable current mode theory at 77°K is tunneling. Therefore, at 77°K the slope of the log current versus voltage plot should be S_m as expressed in Eq. (C.2). The measured slope, S_m, of the log current density versus voltage characteristic, at 77°K, is presented for typical surface barriers in Fig. 1.11 as a function of the inverse square root of the donor concentration. Also presented is the theoretical value of S_m for tunneling current obtained from Eq. (C.3). It can be seen that agreement is excellent. The predicted values of S_m, were the currents thermionic, would be independent of carrier concentration, and completely off the scale of Fig. 1.11. It is clear, therefore, that current conduction at 77°K is by pure field emission (tunneling).

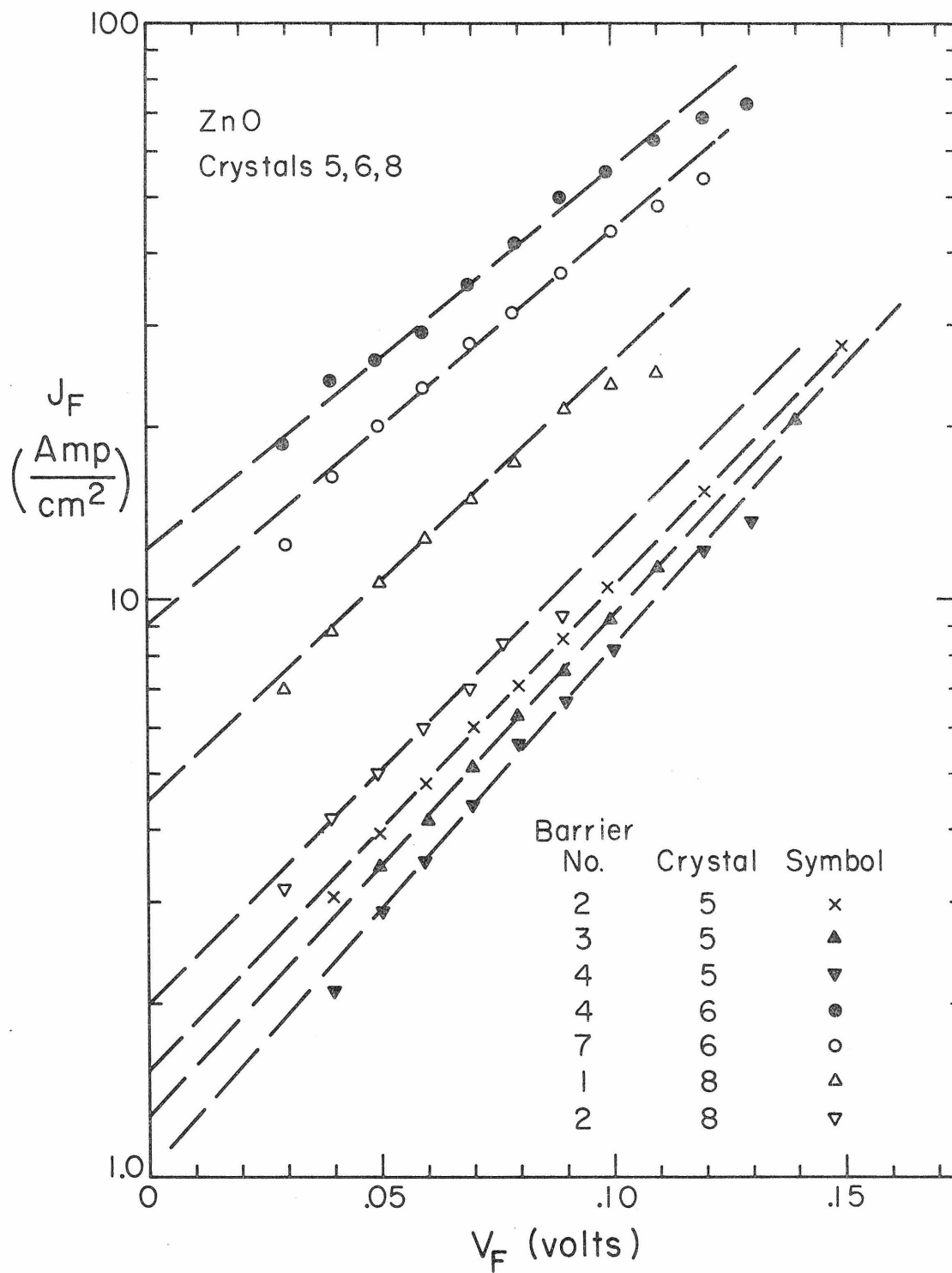Fig. 1.9 The logarithm of the forward current density versus voltage for surface barriers on degenerate zinc oxide at 77°K.
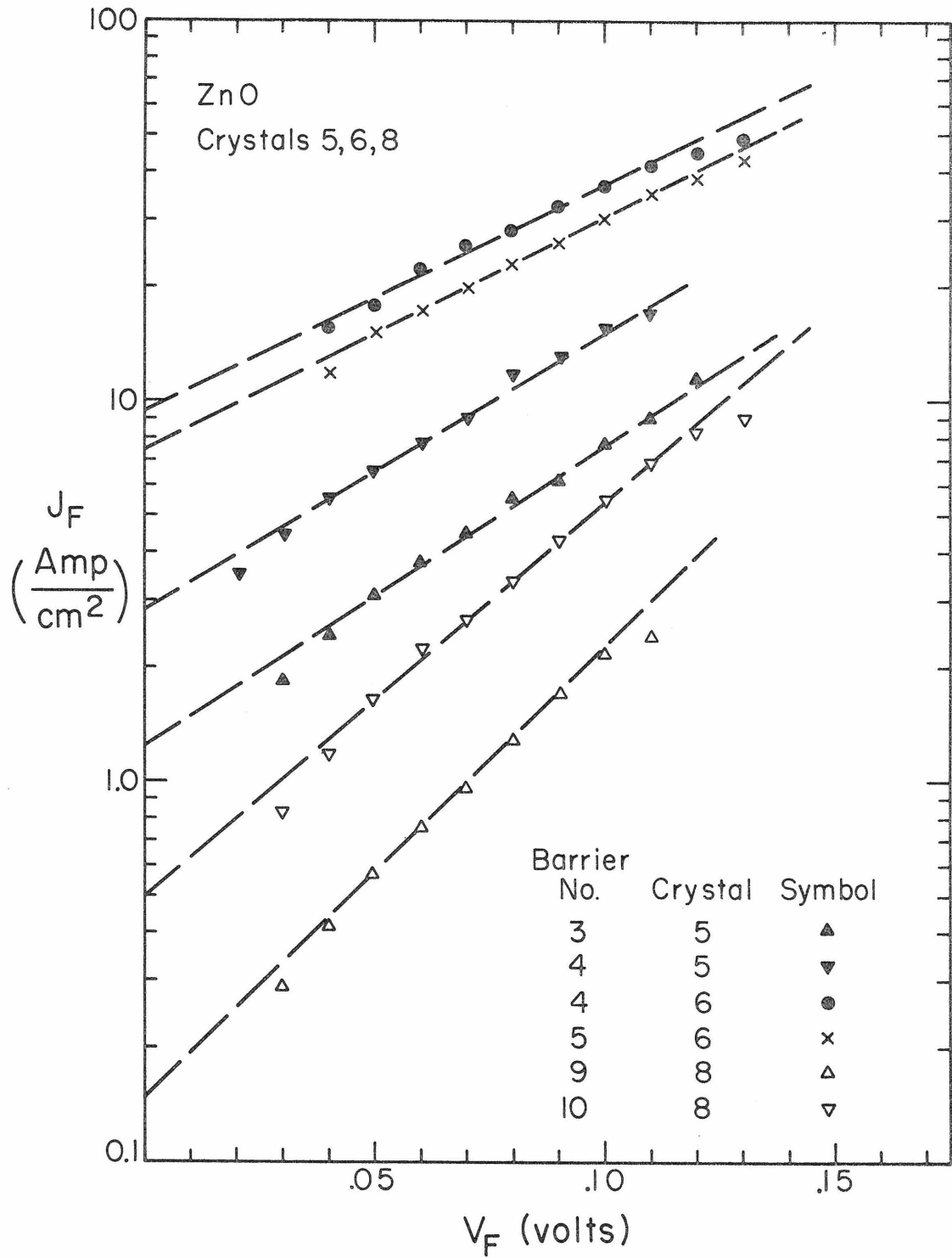
Fig. 1.10 The logarithm of the forward current density versus voltage
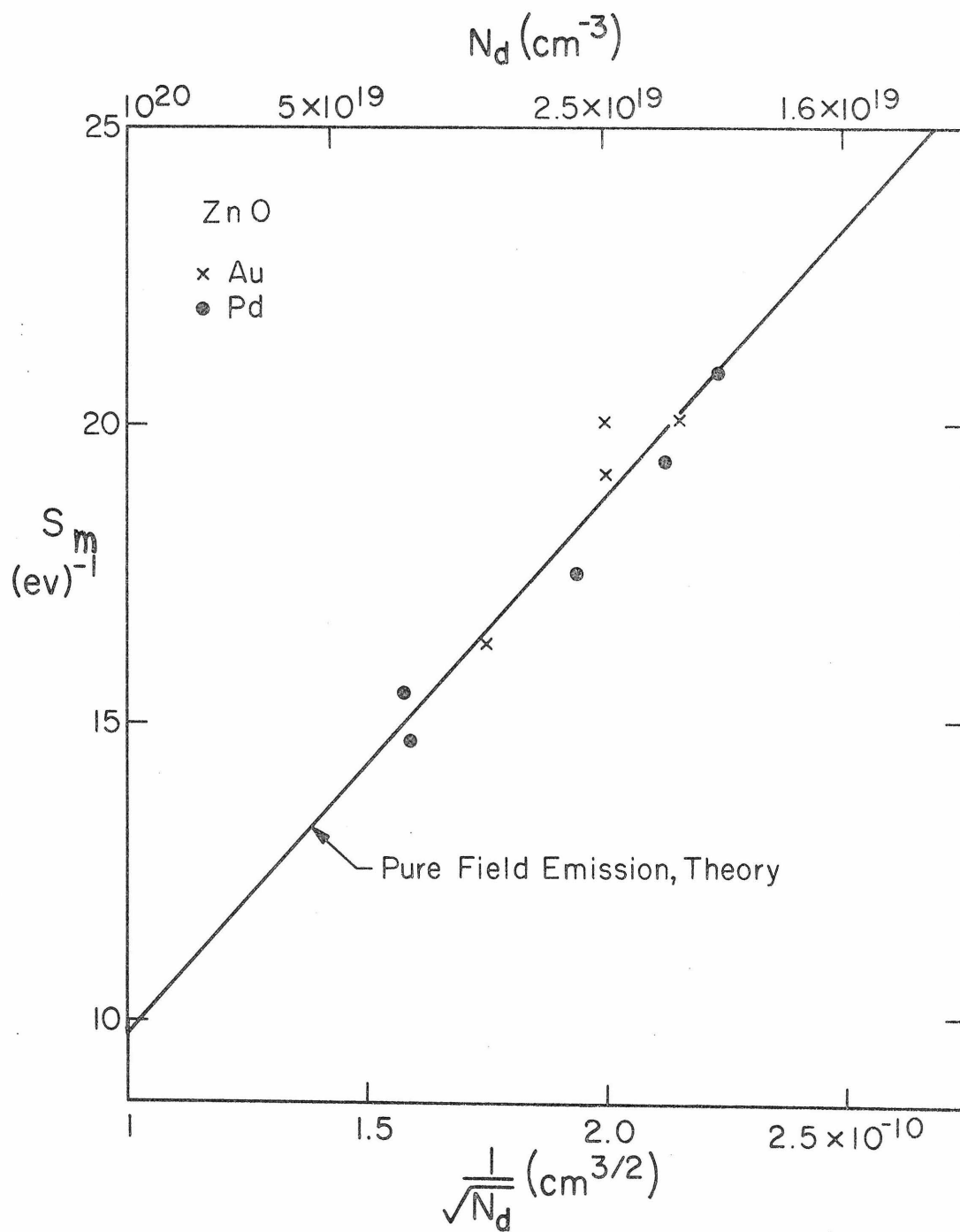for surface barriers on degenerate zinc oxide at 300°K.

Fig. 1.11 Voltage dependence of field emission current for surface barriers on zinc oxide at 77°K as a function of the inverse square root of the impurity concentration.

For the individual surface barrier impurity concentrations used here
the applicable current mode theory at 300°K is thermionic field emission
(TFE). Therefore, at 300°K, the slope of the log current versus voltage
plot will be S as expressed in Eq. (C.12). The measured slope, S, of the
log current density versus voltage characteristic at 300°K is presented
for typical surface barriers in Fig. 1.12 as a function of the inverse
square root of the impurity concentration. Also included is the theoretical
slope, S, for thermionic field emission as calculated from theory using
Eq. (C.12). The quantitative agreement between thermionic field emission
theory and experiment is seen to be excellent. The slope due to pure
thermionic currents at room temperature is 38.4/eV and independent of
carrier concentrations. It is seen that for the concentration range of
interest the currents are not pure thermionic. In conclusion, at 300°K
current conduction through these surface barriers is by thermionic-field
emission.

It has been shown that the surface barrier current conduction is by
tunneling at 77°K and thermionic field emission at 300°K. Therefore, the
extrapolated zero voltage current density, J_o, of typical barriers should
be in accord with tunneling theory Eq. (C.5), at 77°K and thermionic field
theory, Eq. (C.10), at 300°K. In both theories the expected functional
dependence of the zero voltage current density upon the impurity concen-
tration is expected to be approximately linear for the carrier concentra-
tion used. The magnitudes of the current, for both theories, are depen-
dent upon the Richardson constant, A^*, as given in Eq. (A.8). The
effective mass of zinc oxide is 0.38 times the free electron mass. The
Richardson constant is then 4×10^6 A/cm^2 at 300°K and 2.5×10^5 A/cm^2
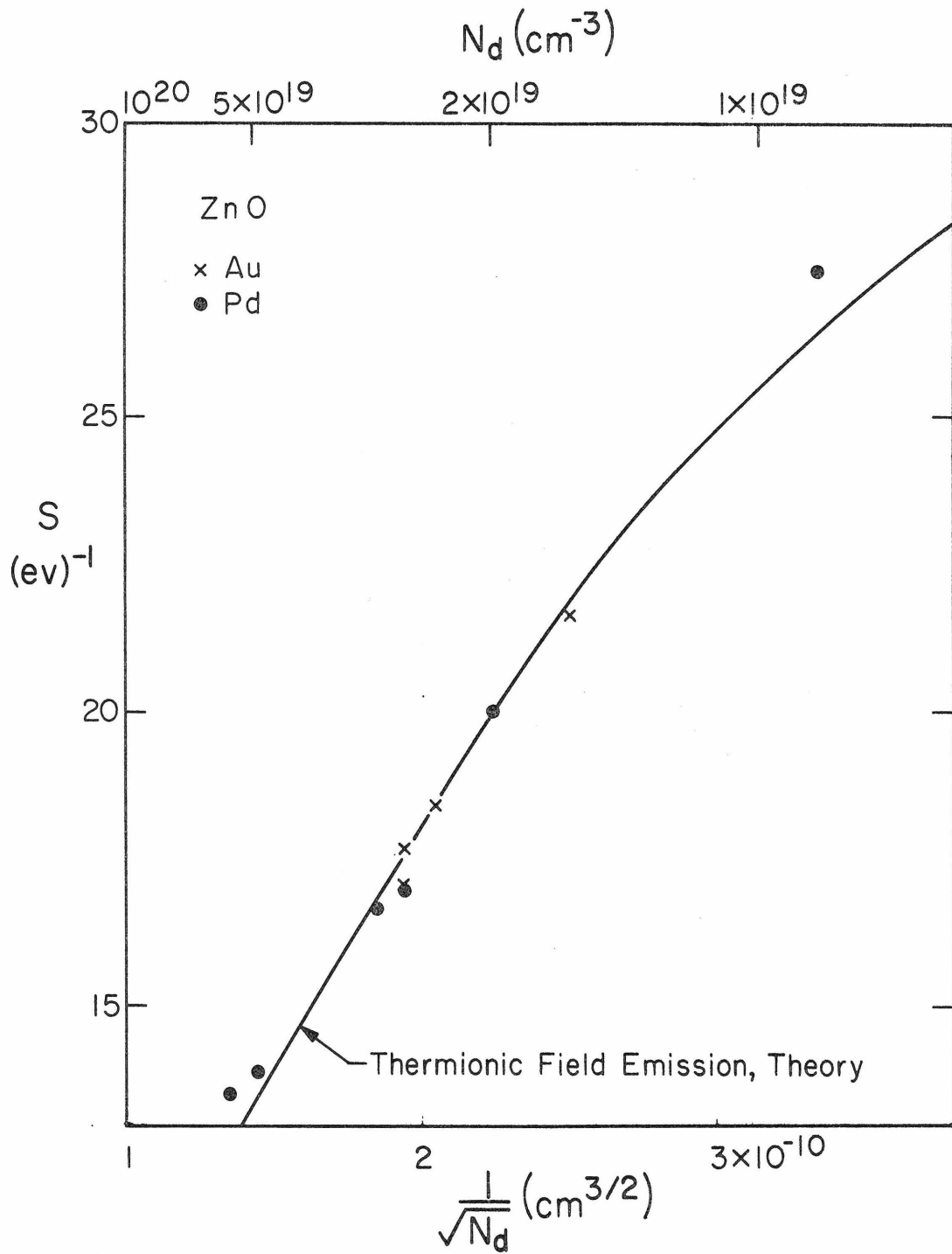
Fig. 1.12 Voltage dependence of field emission current for surface
barriers on zinc oxide at 300°K as a function of the
inverse square root of the impurity concentration.

at 77°K.

The zero-bias extrapolated current density, J_o, at liquid nitrogen temperature is presented as a function of the impurity concentration in Fig. 1.13 for typical barriers. The zero bias current density, as expected from tunneling theory Eq. (C.5) is also presented. The functional dependence in impurity concentrations for theory and experiment is in excellent agreement. However, the value of the Richardson constant which is required for agreement in current magnitude is 2.5×10^4 A/cm^2, a value one-tenth that expected from simple theory and displayed in the preceeding paragraph. The observed current, J_o, then, has the expected functional dependence on impurity concentration but a magnitude one-tenth that expected from theory.

The zero bias extrapolated current density, J_o, at 300°K is presented as a function of the impurity concentration in Fig. 1.14 for typical surface barriers. The zero bias current density, as expected from thermionic field emission theory, Eq. (C.10) is also presented. The functional dependence on impurity concentration for theory and experiment is in excellent agreement. However, the value of the Richardson constant which is required for agreement in current magnitude is 4×10^5 A/cm^2, a value one-tenth that expected from simple theory. The observed current, J_o, then, has the correct functional dependence on impurity concentration but a magnitude one-tenth that expected from theory.

The voltage dependence of tunneling, S_m, and the thermionic field emission currents, S, for surface barriers on degenerate zinc oxide, have been found to agree well with theory. The zero bias currents have been shown to display the theoretically expected functional dependence

Fig. 1.13   The log of extrapolated zero voltage current intercept for
surface barriers on zinc oxide at 77°K as a function of
carrier concentration.   The solid curve is based on
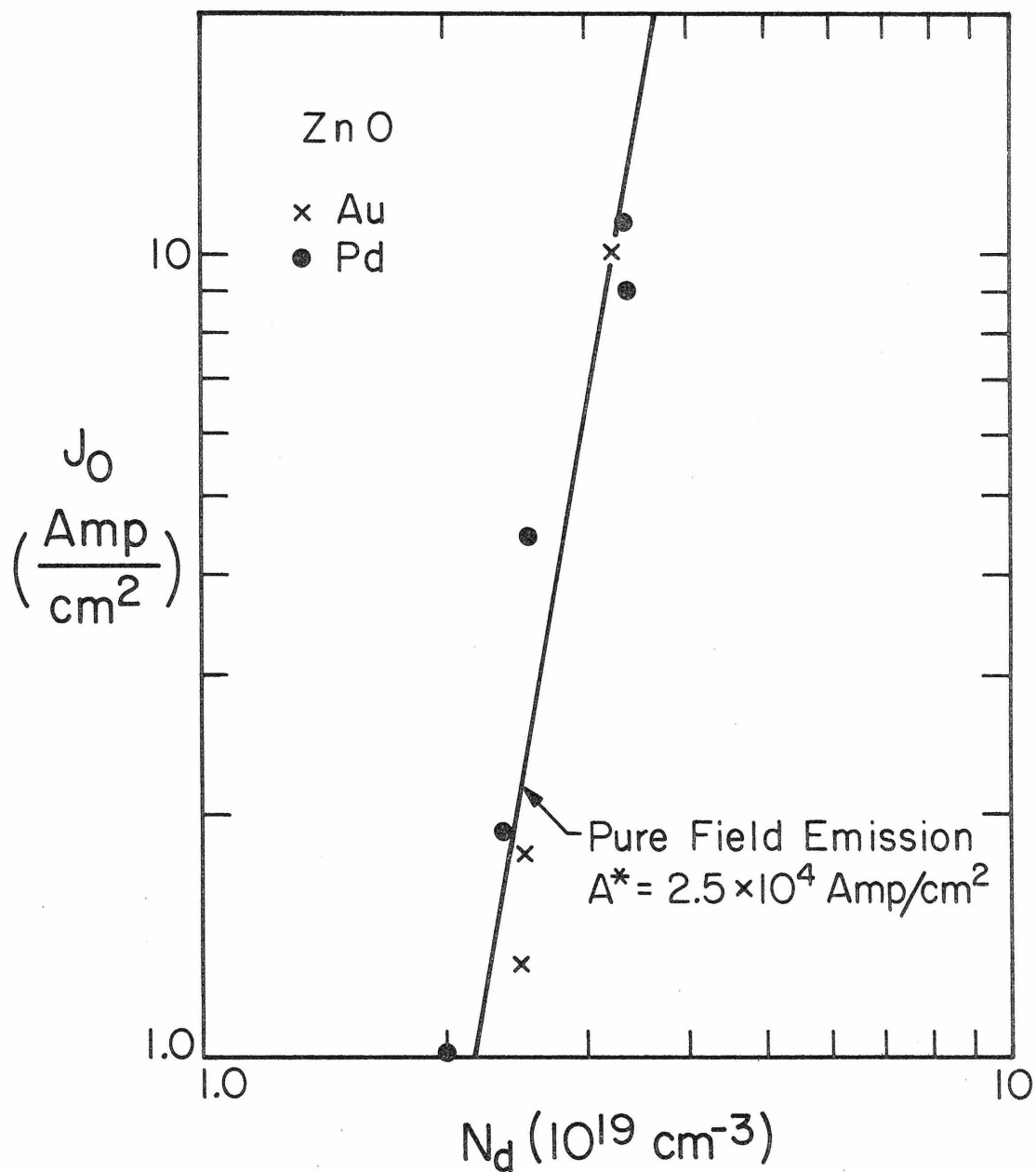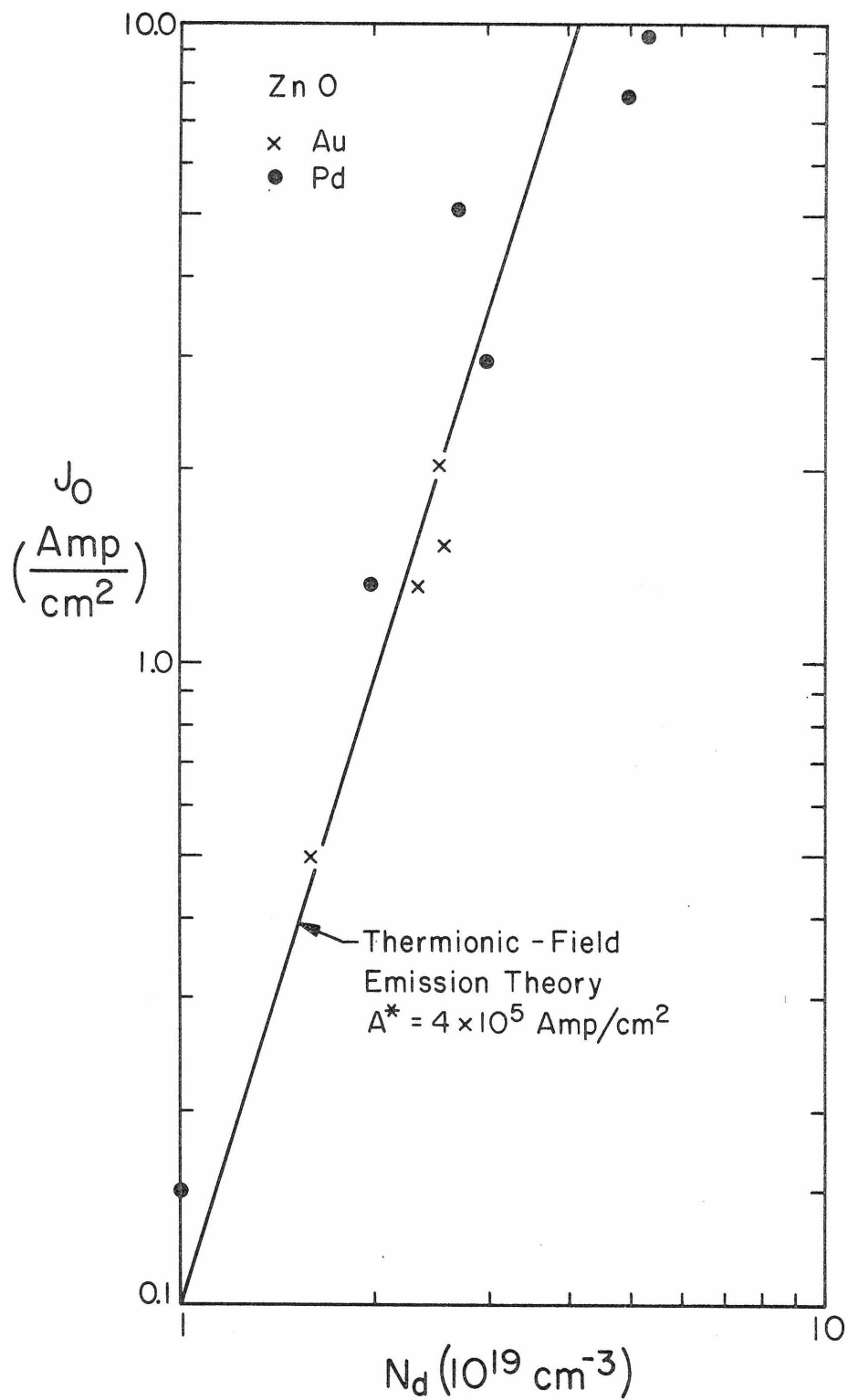tunneling theory in Appendix C.

Fig. 1.14 The log of extrapolated zero voltage current intercept for surface barriers on zinc oxide at 300°K as a function of carrier concentration.

on impurity concetration. However, measurements of zero bias tunneling
and thermionic field emission currents have resulted in measured current
magnitudes which are an order of magnitude less than that predicted by
the appropriate theories. These theories involve the use of the WKB
approximation for tunneling probability[27] and depend on the effective
mass of the charge carrier both in the voltage dependence, S_m and S, and
in the pre-exponential factor, J_o. A second order correction to the
WKB approximation involves only the pre-exponential factor and would
reduce the current density. It is reasonable to suggest, therefore, that
such a correction for effective mass of the electrons might account for
the current descrepancy.

1.7 Zinc Oxide - Conclusions

The current-voltage characteristic on non-degenerate zinc oxide was
found to be in excellent quantitative agreement with simple Bethe diode
theory as modified by image force lowering. The surface barrier energies,
as obtained by photoresponse, current versus voltage, thermal activation
energy and capacitance variation with voltage techniques, were found to
be 0.66 eV for gold and 0.60 eV for palladium. The overall effect is of
a non-degenerate material whose current voltage characteristics are a
"textbook" example.

For indium doped degenerate zinc oxide the slope of the log current
density versus voltage characteristic was found to agree with tunneling
theory at liquid nitrogen temperature and with thermionic field emission
theory at 300°K. The functional dependence of the pure tunneling and
thermionic field emission currents were found to agree with theory at

77°K and 300°K but the absolute magnitudes were less, by an order of magnitude, than that predicted by simple theory. It is suggested that the magnitude effect is a result of the heavy effective electron mass of zinc oxide and theoretical deficiencies.

In the course of this investigation, the existence of traps in the forbidden gap for non-degenerate material was demonstrated. From capacitance measurements trap density was estimated to be approximately one-tenth the effective donor concentration or in the range 2×10^{15} – $2 \times 10^{16}/cm^3$ for the crystals studied. The trap level was estimated to lie between 0.8 and 1.0 eV below the conduction band edge.

Chapter 2

Strontium Titanate

2.1 Introduction

Known for only a relatively few years, strontium titanate is becoming
increasingly important as a synthetic gem stone and, in combination with
barium titanate, as the dielectric material in high value capacitors[28].
Strontium titanate is a member of the peroskvite family of compounds with
a cubic structure at room temperature[29] consisting of a titanium atom
at the center of the cube, oxygen atoms on the faces and strontium atoms
at the corners. As the temperature is decreased the crystal structure
becomes tetragonal at 110°K, orthorhombic at 65°K and rhombohedral at
10°K[29]. Electrically it is an insulator when pure with a room tempera-
ture band gap of 3.15 eV[30]. Upon reduction by heating in a hydrogen
atmosphere the clear colorless insulating crystal becomes an n-type
semiconductor and the color becomes a varying shade of blue as a result
of free carrier absorption[31]. Little has been done with the reduced
material except some studies of the mobility conducted by a number of
authors[32-35] at temperatures between 300°K and 4.2°K with some varia-
tion in results.

Even though it is used extensively in capacitors no systematic
study of the relative permittivity of strontium titanate has been conducted.
Reported studies have been inconsistent as to the exact behavior as a
function of temperature, electrical bias and frequency of measurement.

At room temperature the reported value of the relative permittivity for strontium titanate lies between 307 and 370 [36,37]. At 77°K the reported relative permittivity lies between 1600[38] and 2000[39,40]. Rupprecht[41] reports that the relative permittivity is independent of the measurement frequency from 1 KHz to 26 GHz between 93°K and 300°K. Itschner and Gränicher[42] report field strength independence of the relative dielectric constant for fields up to 10^6 V/cm above 110°K. At elevated temperatures the relative permittivity follows a Curie-Weiss law temperature variation[39,40,43,44] with the reported Curie temperature between 28°K and 44°K. Some authors[34,35] have reported narrow hysteresis loops characteristic of a ferroelectric material at temperatures below the Curie point. Others[46] have found no evidence of ferroelectricity. At liquid helium temperature (4.2°K) there is a wide range in reported values of the relative permittivity. Values from 1300 to well in excess of 20,000 have been reported[37,38,39,40,42,45] under a wide range of applied bias field and measurement frequencies.

The surface barrier energies of strontium titanate are not known. To understand a semiconductor it is essential that the surface barrier energies on both vacuum cleaved and chemically prepared surfaces be known. To understand the properties of strontium titanate as a capacitor dielectric it is essential that the relative permittivity be known as a function of temperature and applied electric field strength.

A systematic intensive investigation of the surface barrier properties of strontium titanate and into the relative permittivity of this material was conducted. Samples of strontium titanate were reduced in a hot hydrogen atmosphere. The bulk resistivity and mobility of the

non-degenerate reduced crystals were determined as a function of temperature and carrier concentration. A complete and systematic study of the metal-semiconductor Schottky barrier systems represented by gold, palladium, copper, and indium surface barriers on both cleaved and chemically prepared strontium titanate surfaces was made using photoresponse, forward current-voltage characteristics, thermal activation energy, and capacitance variation with voltage techniques. Values obtained by use of the first three techniques were found to be in good agreement. However, surface barrier energies obtained from capacitance variation with voltage proved to be meaningless, with both excessive scatter within the individual set of data and incomprehensible behavior as compared to the other barrier measurements. Forward and reverse current-voltage characteristics were studied and analyzed in terms of simple Bethe diode theory[9] as modified by image force lowering. The value of the diode non-ideality factor obtained was twice that predicted by image force lowering. Both the capacitance and current effects could be due to some effect of the dielectric constant.

The systematic investigation into the relative permittivity was conducted in order to obtain an accurate description of the behavior of the dielectric constant as a function of temperature from 4.2°K to 300°K. Using the strontium titanate as the dielectric in a capacitor, measurements of the relative permittivity were obtained as a function of frequency, temperature, and applied DC field. A careful search was made for evidence of ferroelectricity although none was found. A phenomonological expression for the free energy of the crystal was developed which permits the description of the energy-distance relationship for the

titanium atom. Measurements of the relative permittivity at frequencies above 10^5 Hz and at temperatures below 65°K were observed to be anomalous with the value of relative permittivity being a function of past electrical stresses. This behavior was traced to domain effects in the crystal.

At the end of these investigations a knowledge of the surface barrier energies on both chemically prepared and cleaved strontium titanate had been obtained. The study of the relative permittivity yielded a phenomonological model describing the permittivity of strontium titanate and giving information concerning the free energy of the titanium atom.

2.2 Description and Preparation of the Material

The starting material was a clear colorless boule with a resistivity in excess of 10^{11} ohm-cm. Using a diamond saw the boule was sliced into thin wafers 1.5 mm thick in a direction parallel to the (100) faces. From these wafers samples were prepared for measuring the dielectric properties of strontium titanate and for measuring surface barrier properties.

The four sample wafers to be used in the dielectric investigations were hand lapped and polished on a succession of silk cloths starting with an 800 mesh grit, progressing through 1200 and 3200 grits, 1 μ and .3 μ polishing compound and finishing with a 500 Å alumina polishing compound. Final wafer thickness was between 0.125 mm and 1 mm with wafer orientation yielding two large flat surfaces in the (100) crystalline planes. The wafer surfaces were cleaned by etching in phosphoric acid for ten minutes, followed by immersion in hydrochloric acid for ten minutes to remove phosphates. After a fifteen minute rinse in flowing deionized water the four samples were dried in a jet of dry, filtered air.

Capacitors with strontium titanate as the dielectric were formed, by placing them in an ion pumped evaporator at a nominal pressure of 8×10^{-7} Torr and evaporating a layer of gold, 3000 Å thick, from a hot tungsten filament, on one side of each slice. The wafers were withdrawn from the evaporator, inverted, and replaced in the vacuum. Approximately 2000 Å of gold was then evaporated through a large mesh screen to form a contact. Contact diameters from 0.1 to 1.0 cm were used, taking care that the diameter was much greater than the sample thickness to avoid fringe capacitance effects.

Other wafers for use in Hall, resistivity and surface barrier measurements were hand lapped and polished in the same fashion as were the dielectric samples. The nominal thickness for these samples was 1 mm. Using a diamond wire saw these wafers were cut into six sample bars whose dimensions were approximately 1 x 2 x 10 mm. These bars were cleaned by etching in phosphoric acid and hydrochloric acid, rinsing in water and air drying in the same manner as the dielectric sample wafers.

To determine the purity of the material and confirm the information furnished with the boule by the manufacturer, National Lead Company, sample bar number 4 was submitted to the Geology Department of the California Institute of Technology for an impurity analysis. There Dr. A. Chodos performed a semi-quantitative analysis using an electron microprobe. Principal impurities found were 0.0002 percent barium, 0.01 percent calcium oxide, and less than 0.1 percent tungsten. These data are in agreement with that furnished by the manufacturer.

On an individual basis the remaining 5 sample bars were placed in a purified hydrogen furnace at a pressure of 1.5 psi and heated for the

time and temperature indicated in Table 2.1. In this manner sample bars with a range of electron concentrations between 10^{16} and 7×10^{17} per cm^3 were obtained, since the process creates oxygen vacancies which act as donors[47]. The crystal bars, as a result of free carrier absorption[47] now ranged in color from pale blue to black. Leads were soldered to the samples using a low melting 10% silver-90% indium solder and Hall and resistivity measurements were made. Next the samples' surface layers were removed by soaking for ten minutes in hydrochloric acid, to remove the solder, ten minutes in 50°C phosphoric acid and ten minutes in hydrochloric acid. The sample bars were rinsed in deionized water for fifteen minutes and dried in a jet of dry filtered air. Gold, palladium, copper, or indium barriers were evaporated through a fine screen onto the polished, chemically cleaned surface in an ion-pumped vacuum with a nominal pressure of 5×10^{-7} Torr. Nominal barrier diameter was 100 μ. Two leads were soldered onto the crystal bulk using 90% indium-10% solder and a contact made to the barrier by a gold wire. Current, voltage, and capactiance measurements were made.

An additional series of barrier measurements were performed on cleaved samples. The five sample bars used for barrier measurements on chemically prepared surfaces were reused. Each sample bar was cleaved in a vacuum in a stream of evaporating gold, palladium, copper, or indium. Barrier area and sample lead configuration were similar to the chemically prepared surface barrier devices. Each sample bar was cleaved at least twice while evaporating a different metal for each cleave.

Crystal	1	2	3	5	6	
Preparation						
Temperature	770	750	750	795	830	°C
Atmosphere	1.5	1.5	1.5	1.5	1.5	PSI-hydrogen
Time	240	180	10	240	420	Minutes
Room Temperature Values						
Resistivity	11.8	27.1	39.6	1.36	.300	ohm-cm
Mobility	7.35	8.85	8.95	26	31.8	cm^2/volt-sec
Carrier Concentration	7.15	3.10	2.00	17	66.0	$10^{16} cm^{-3}$ (±10%)
Liquid Nitrogen Temperatures						
Resistivity	4.05	13.3	45.0	2.04	.136	ohm-cm
Mobility	55	62	63.7	162	195	cm^2/volt-sec
Carrier Concentration	2.8	.76	.206	1.9	27.2	$10^{16} cm^{-3}$ (±10%)
Liquid Helium Temperatures						
Resistivity	7.2	10.4	29.4	2.72	0.83	ohm-cm
Mobility	1200	2000	2100	4000	5000	cm^2/volt-sec
Carrier Concentration	7.2	3	1.0	5.8	15	$10^{14} cm^{-3}$ (±20%)

Table 2.1

Bulk Resistivity and Mobility Measurements

on Typical Strontium Titanate Samples

2.3 Bulk Measurements

Resistivity measurements were made using an electrometer on five sample bars cut from the original boule. The intrinsic resistivity of these bars was determined to be in excess of 10^{11} ohm-cm. The stoichiometry of the original bars was altered by reduction. This made samples available for study with differing carrier concentrations.

Hall and resistivity measurements were made on all samples after reduction using a battery current source, a picoammeter, and two digital voltmeters. Table 2.1 presents Hall and resistivity measurements on the samples at typical temperatures. A 4.7 kilo Gauss magnet was employed for the measurements. The effective carrier concentration was obtained using Eq. 1.1

In Fig. 2.1 the Hall mobility versus temperature is presented for several samples. The temperature dependence of the mobility above a temperature of 40°K is consistent with single phonon scattering[16]. Below this temperature the temperature dependence of the mobility is seen to decrease, due to impurity scattering.

At room and liquid nitrogen temperatures the values of mobility obtained for the more lightly doped samples (1,2,3) are in agreement with those obtained by Frederiske et al.[32-]. The mobilities found for samples 5 and 6 are factors of three to four higher. The liquid helium temperature values of mobility are in agreement with those obtained by Frederiske[33,34] and by Tufte and Chapman[35]. The high mobility of the more heavily doped samples is consistent with annealing of scattering centers during the reduction process used to create the donors.
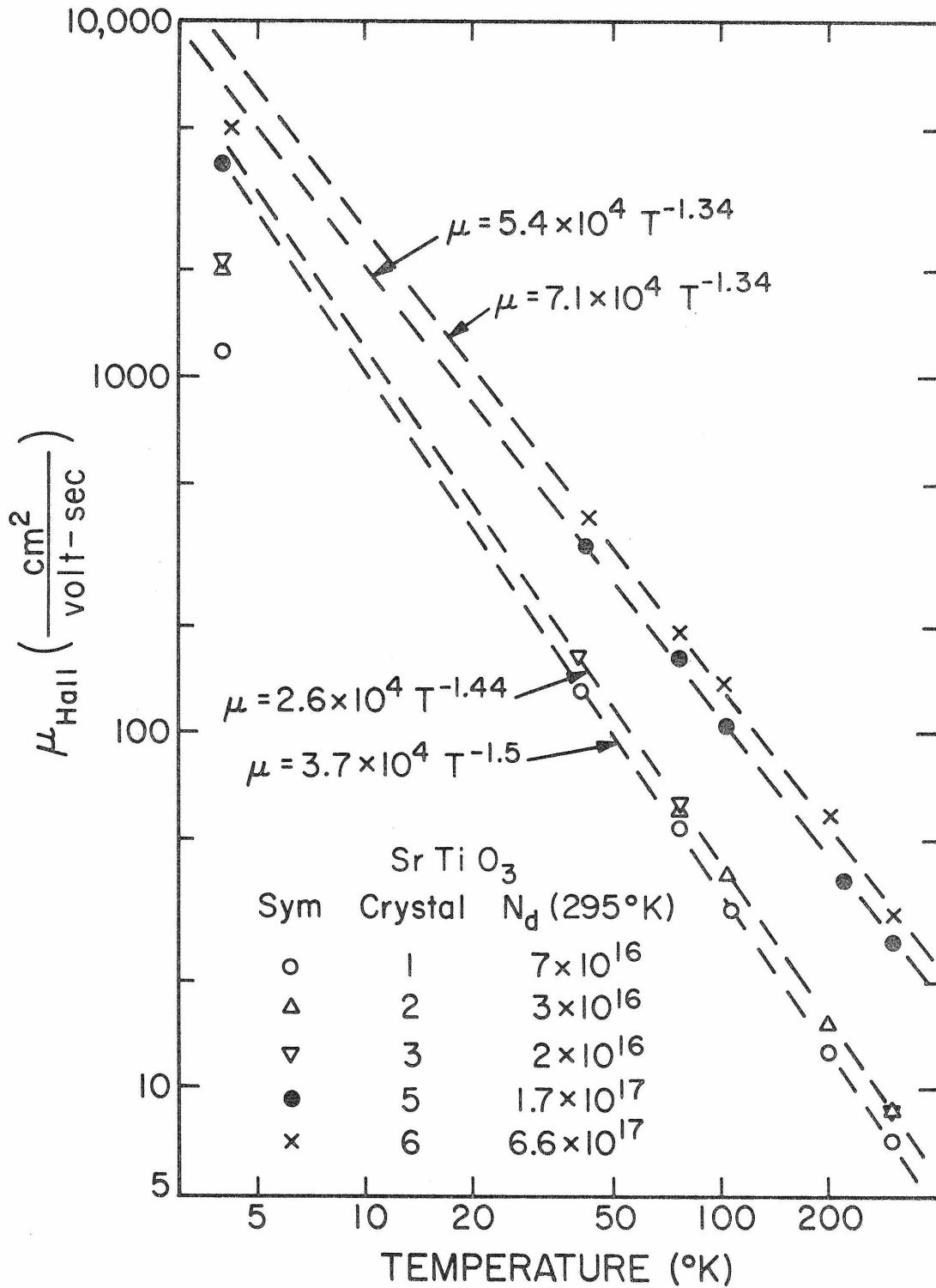
Fig. 2.1 The logarithm of the mobility versus the logarithm of the temperature for reduced strontium titanate samples.

2.4 Surface Barrier Measurements

The properties of gold, palladium, copper, and indium surface barriers on both chemically prepared and on cleaved strontium titanate surfaces were investigated. Barrier energies were measured using photoresponse, current-voltage characteristics, thermal activation energy techniques and the capacitance variation with voltage. A detailed discussion of these methods is held in Chapter 1 and, in Appendix A, the pertinent computational methods are outlined.

2.4.1 Photoresponse

The surface barrier energy was determined by a measurement of the short circuit photocurrent using light entering the crystal from the barrier contact surface (a front-wall configuration). A tungsten-halide lamp was used in conjunction with a Gaertner quartz-prism monochrometer. The light was chopped at 50 Hz and a lock-in amplifier was used to improve the signal-to-noise ratio.

In Fig. 2.2 typical photoresponse is presented for gold, palladium, copper, and indium surface barriers on chemically prepared strontium titanate surfaces. In Fig. 2.3 typical photoresponse data for gold, palladium, copper, and indium surface barriers on cleaved strontium titanate surfaces is represented. Photoresponse data on both chemical and cleaved surface barriers are linear in accord with theory[17]. At high photon energies surface scattering and impurity absorption reduce the response. To determine the effect of carrier concentration on barrier energy, several sample bars were used for each type of metal barrier. No indication of any effect of carrier concentration was observed. Surface
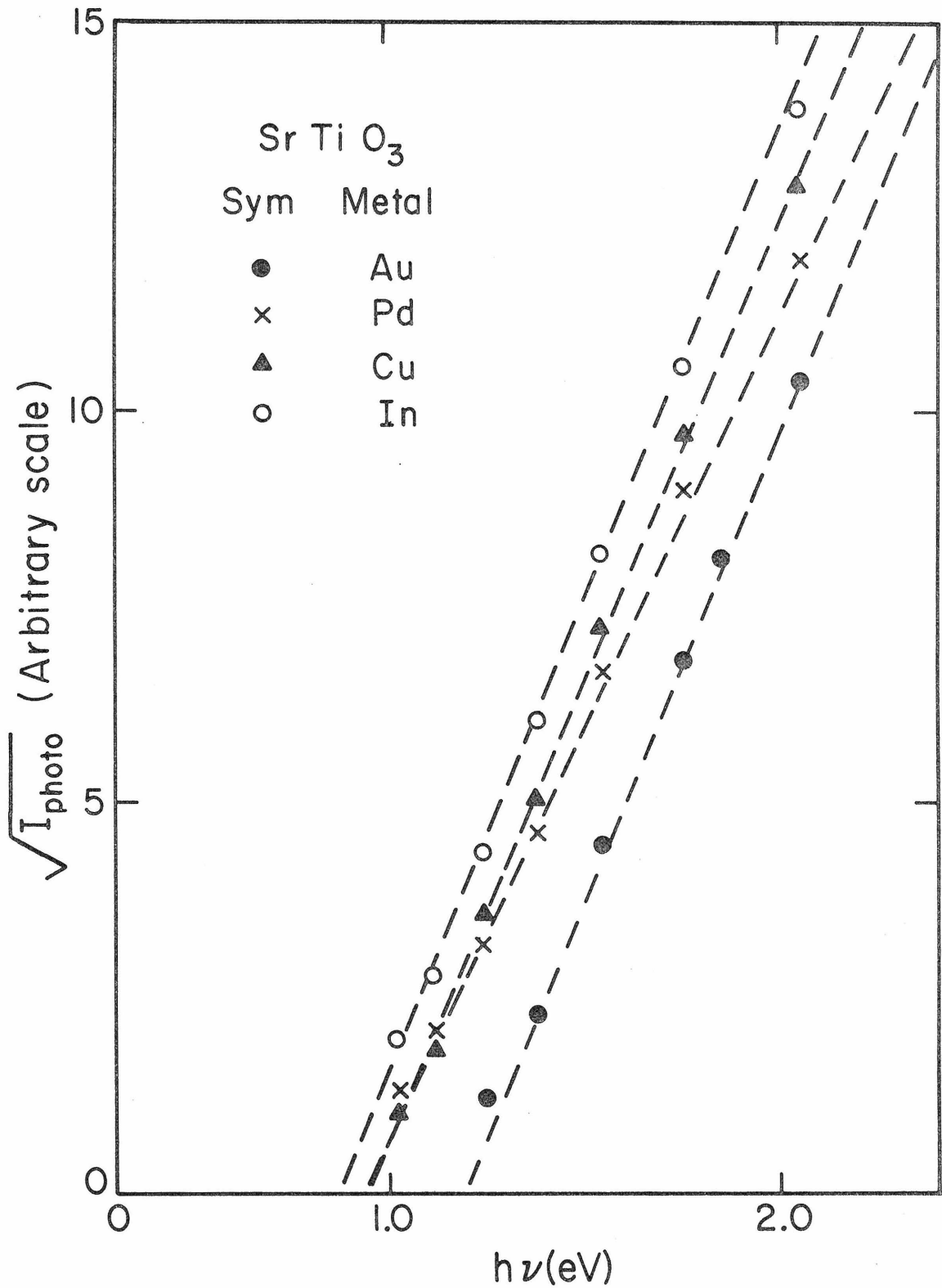
Fig. 2.2 Square root of photo current per incident photon versus photon
energy for surface barriers on chemically prepared strontium
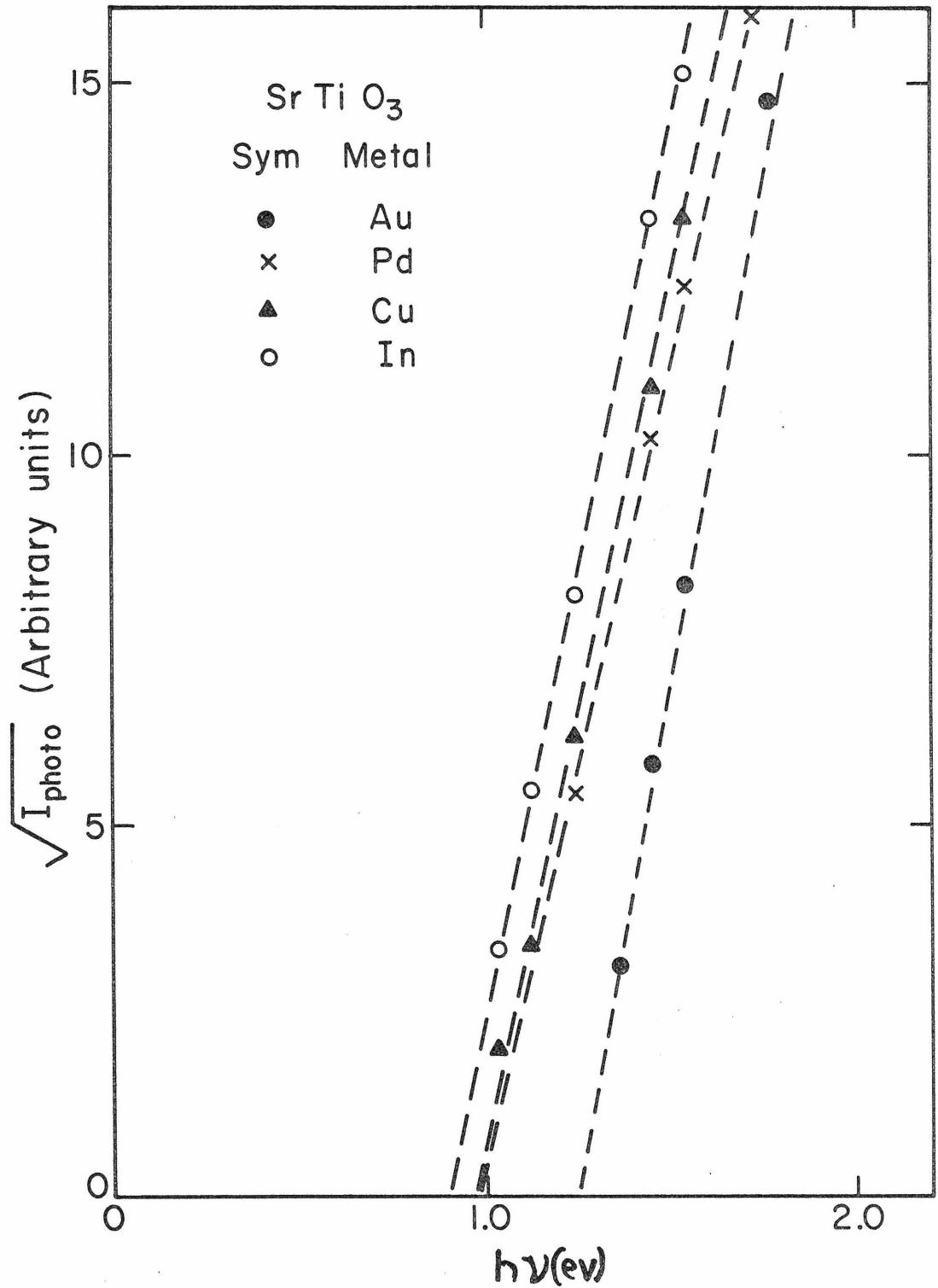titanate at 300°K.

Fig. 2.3 Square root of photo current per incident photon versus photon
energy for surface barriers on cleaved strontium titanate at
300°K.

barrier energies as determined by photoresponse are listed in Table 2.2 for both chemically prepared and vacuum cleaved surfaces.

2.4.2 Forward Current - Forward Voltage

Typical curves of the forward current density versus forward voltage characteristics are presented in Fig.s 2.4 and 2.5 for gold, palladium, copper, and indium surface barriers on chemically prepared and vacuum cleaved surfaces. The individual surface barrier areas were approximately 8×10^{-5} cm^2. The same crystals were used as for photoresponse measurements to facilitate comparison of the measurements. The current was supplied by a battery in combination with a variable resistor. Voltages were measured with a Darcy digital voltmeter and currents were measured using a EGG picoammeter. The measurements were made in darkness to eliminate effects of generation-recombination current.

The straight line behavior of the logarithm of current density as a function of applied voltage over three orders of magnitude is in excellent agreement with thermionic theory (Appendix A). The effects of excess series resistance are seen at high currents and reverse currents reduce current density at small voltages. The slope of the log current versus voltage is experimentally measured to be 63.7 mV per decade of current. The extrapolated zero voltage current intercept provides the basis for the calculation of the barrier energy as outlined in Appendix A.

Barrier Energy

(Electron Volts)

Technique	Photoresponse	I-V Characteristic	Activation Energy	Average
-----------------------------------Chemically Prepared Surface------------------------------------				
Gold	1.20 ± .06	1.16 ± .05	1.22 ± .06	1.19 ± .06
Palladium	0.94 ± .04	0.97 ± .05	1.01 ± .05	0.97 ± .05
Copper	0.95 ± .05	0.89 ± .04	0.95 ± .05	0.93 ± .04
Indium	0.87 ± .03	0.86 ± .025	0.87 ± .04	0.87 ± .03
---Cleaved Surface---------------------------------------				
Gold	1.25 ± .03	1.17 ± .07	1.26 ± .08	1.23 ± .07
Palladium	0.98 ± .02	1.02 ± .05	1.05 ± .04	1.02 ± .04
Copper	0.97 ± .03	0.92 ± .04	0.97 ± .02	0.95 ± .03
Indium	0.90 ± .022	0.90 ± .013	0.90 ± .022	0.90 ± .02

TABLE 2.2

Surface Barrier Energies
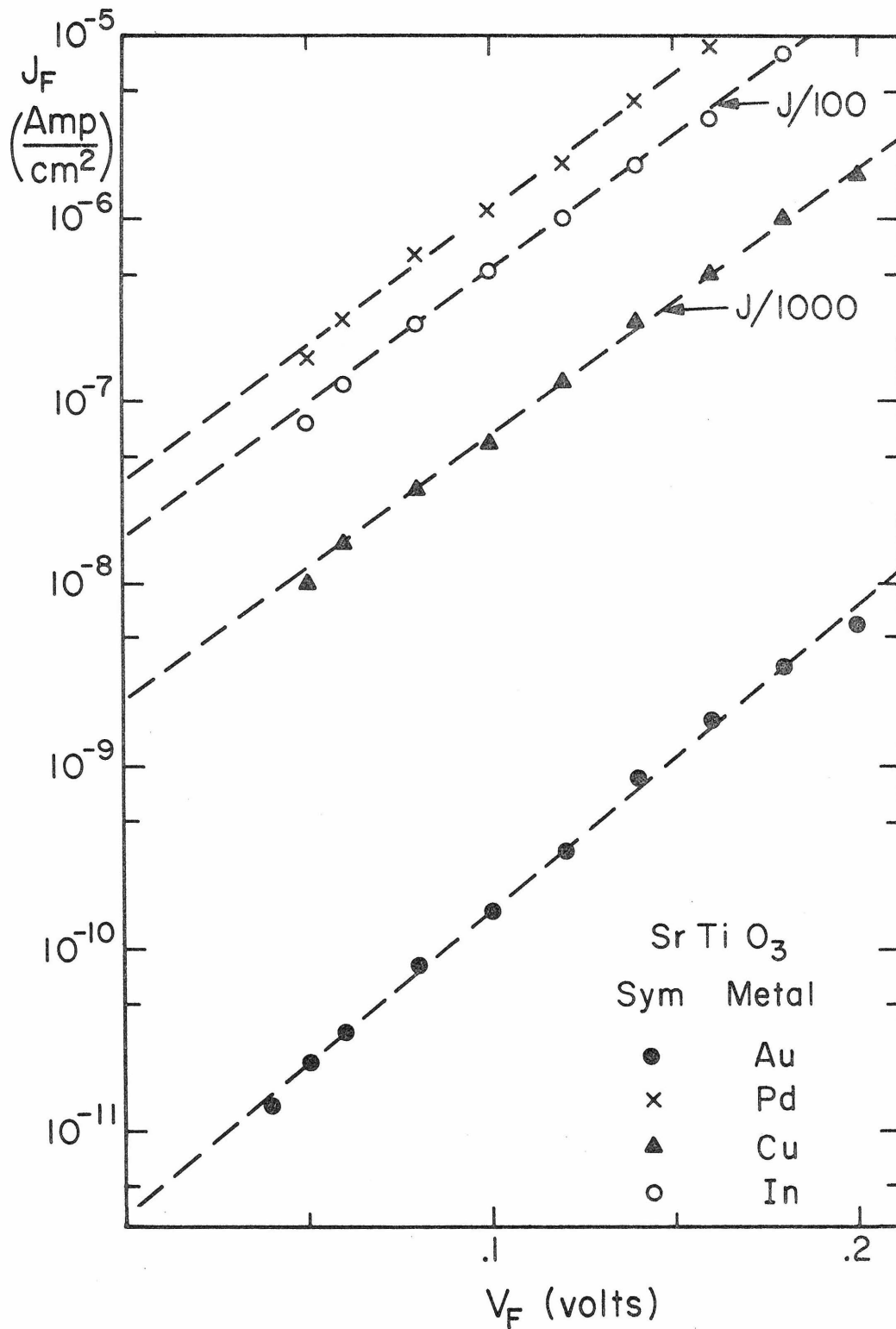
on Strontium Titanate

Fig. 2.4   The logarithem of the forward current density versus voltage
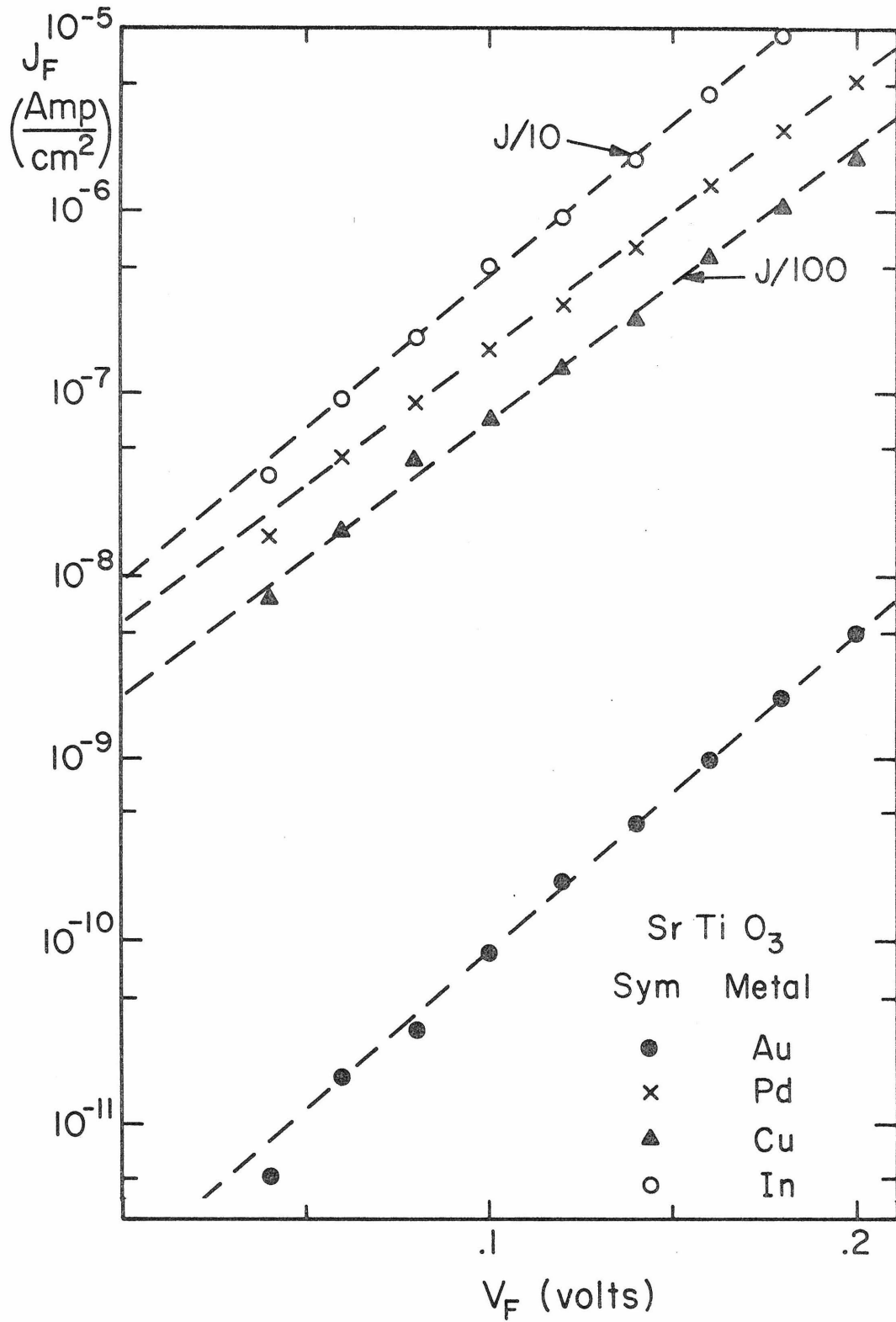for surface barriers on chemically prepared strontium titanate
at 300°K.

Fig. 2.5   The logarithm of the forward current density versus voltage
for surface barriers on cleaved strontium titanate at
300°K.

2.4.3 Thermal Activation Energy

Typical curves of the logarithm of the normalized reverse current as a function of the inverse temperature are displayed in Fig. 2.6 for surface barriers on chemically prepared strontium titanate and in Fig. 2.7 for surface barriers on cleaved strontium titanate. The barriers were biased at − 1 volt using a battery operated power supply and the measurements were made using an electrometer and a digital voltmeter. Temperature variation was accomplished using a Peltier cooler-heater and the measurements were made in the dark to minimize generation-recombination current. Repeatability of the measurement was ± 2% with the exception of the 13°C measurements on gold and the 7°C measurements on palladium. There a range in observed currents gives rise to some uncertainty. The straight line of the log current versus inverse temperature display is expected from simple diode theory (Appendix A). The observed current magnitudes of the reverse current at room temperature were in the 10^{-7} to 10^{-12} ampere range.

2.4.4 Capacitance Barrier Measurements

An attempt was made to measure the barrier energy by extrapolating to zero voltage the plot of $1/C^2$ as a function of the bias voltage on all barriers for which barrier energies were measured by the other methods.

The capacitances were measured at room temperature using a bridge with a frequency of 10 KHz. Both chemically prepared and cleaved strontium titanate sample surface barriers were measured under no illumination conditions to minimize effects from charged traps. The capacitance change with voltage was much smaller than predicted by theory (Appendix B) and varied unpredicably making barrier prediction by the method impossible.
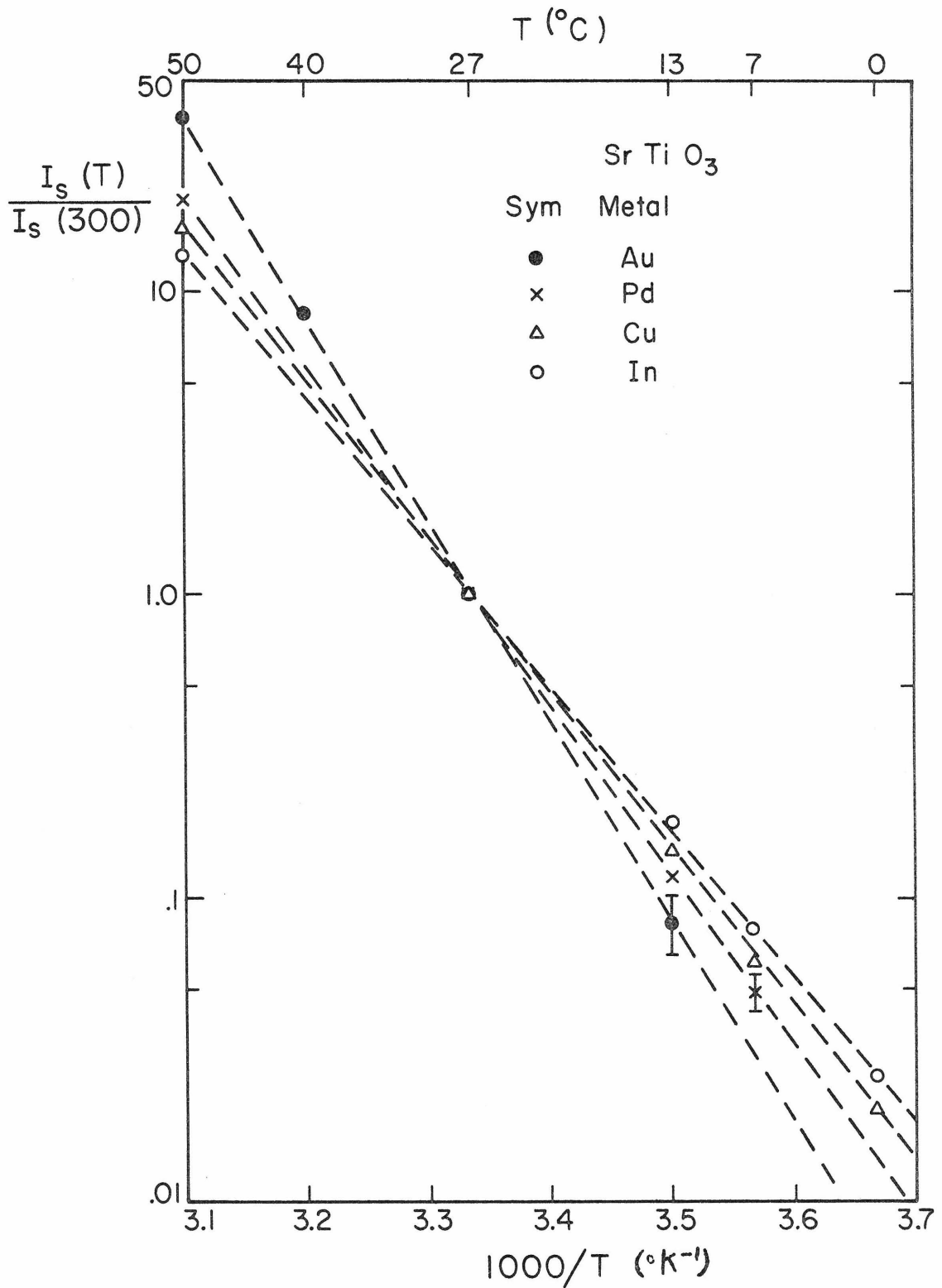
Fig. 2.6 **The logarithm of the noramlized reverse current versus inverse temperature for surface barriers on chemically prepared strontium titanate at -1 volt bias.**
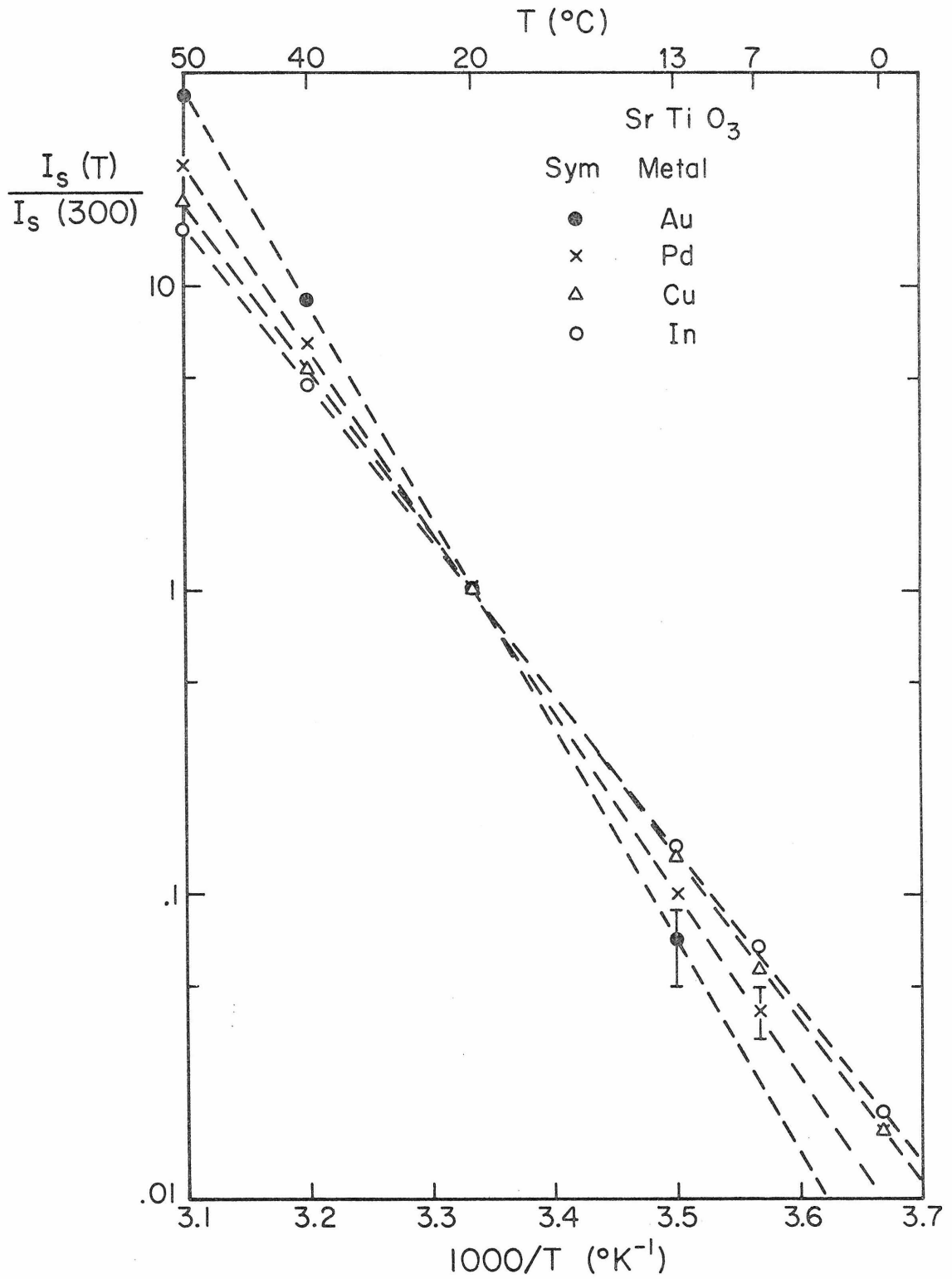
Fig. 2.7 The logarithm of the noramlized reverse current versus inverse temperature for surface barriers on cleaved strontium titanate at -1 volt bias.

2.4.5 Barrier Energy Summary and Discussion

A discussion of the pertinent theories and factors to be considered in determining the surface barrier energies by the various techniques is contained in Chapter 1, Section 4. To summarize, the barrier energy can be obtained from: 1) the extrapolated intercept for zero short-circuit photocurrent in a photoresponse as a function of photon energy plot; 2) the extrapolated zero voltage current density and slope of a log current density versus applied voltage plot; 3) the slope of the log reverse current versus inverse temperature as corrected for change in barrier energy with temperature; and 4) the extrapolated infinite capacitance intercept of the $1/C^2$ versus V plot.

The values of surface barrier energy are presented in Table 2.2 as determined by photoresponse, current-voltage characteristic, and thermal activation energy techniques for gold, palladium, copper, and indium surface barrier diodes. Data for surface barriers on both chemically prepared and cleaved strontium titanate crystal surfaces are included. A minimum of 30 barriers was used for each measurement with each metal. The agreement in surface barrier energies as determined by photoresponse, current-voltage, and thermal activation energy methods is excellent. The slightly lower surface barrier energy values for chemically prepared surfaces is the result of surface states on the material as has been seen in other materials[48]. No consistent variation in surface barrier energy with change in donor concentration was observed by any technique.

The current-voltage characteristics follow simple thermionic diode theory[20] over three orders of magnitude in current before series resistance effects reduce the expected current. The value of n, the diode

non-ideality factor, was found to be 1.07 ± 0.03, using slopes of log cur-
rent versus voltage (Figs. 2.4 and 2.5). This is approximately 1.6 times
that predicted from theory using an optical dielectric constant of 6[50]
but is in agreement with the value of n calculated using a unity optical
dielectric constant.

The barrier capacitance change with applied voltage was variable and
much less than would be predicted by theory (Appendix B). This resulted
in an infinite capacitance intercept and surface barrier energies in
excess of the band gap energy with a large scatter in values. The slope
of the $1/C^2$ versus voltage curve is inversely proportional to the impurity
concentration according to theory (Appendix B). The values of impurity
concentration obtained in this manner were higher by 1 to 20 orders of
magnitude than those obtained from Hall and resistivity measurements.
These meaningless concentration and barrier energy values were discarded.

2.5 Reverse Current-Voltage Measurements

The forward current versus voltage characteristic has been shown to
be consistent with thermionic diode theory[9,20] as modified by image
force lowering of the barrier when the optical dielectric constant is
taken as unity. The observed optical permittivity is 6[50]. Studies
of the reverse current-voltage characteristics were conducted in an inves-
tigation as to whether this dependence on unity optical dielectric con-
stant continued in the reverse direction. Typical normalized reverse
current versus α, where α is the fourth root of the barrier energy less
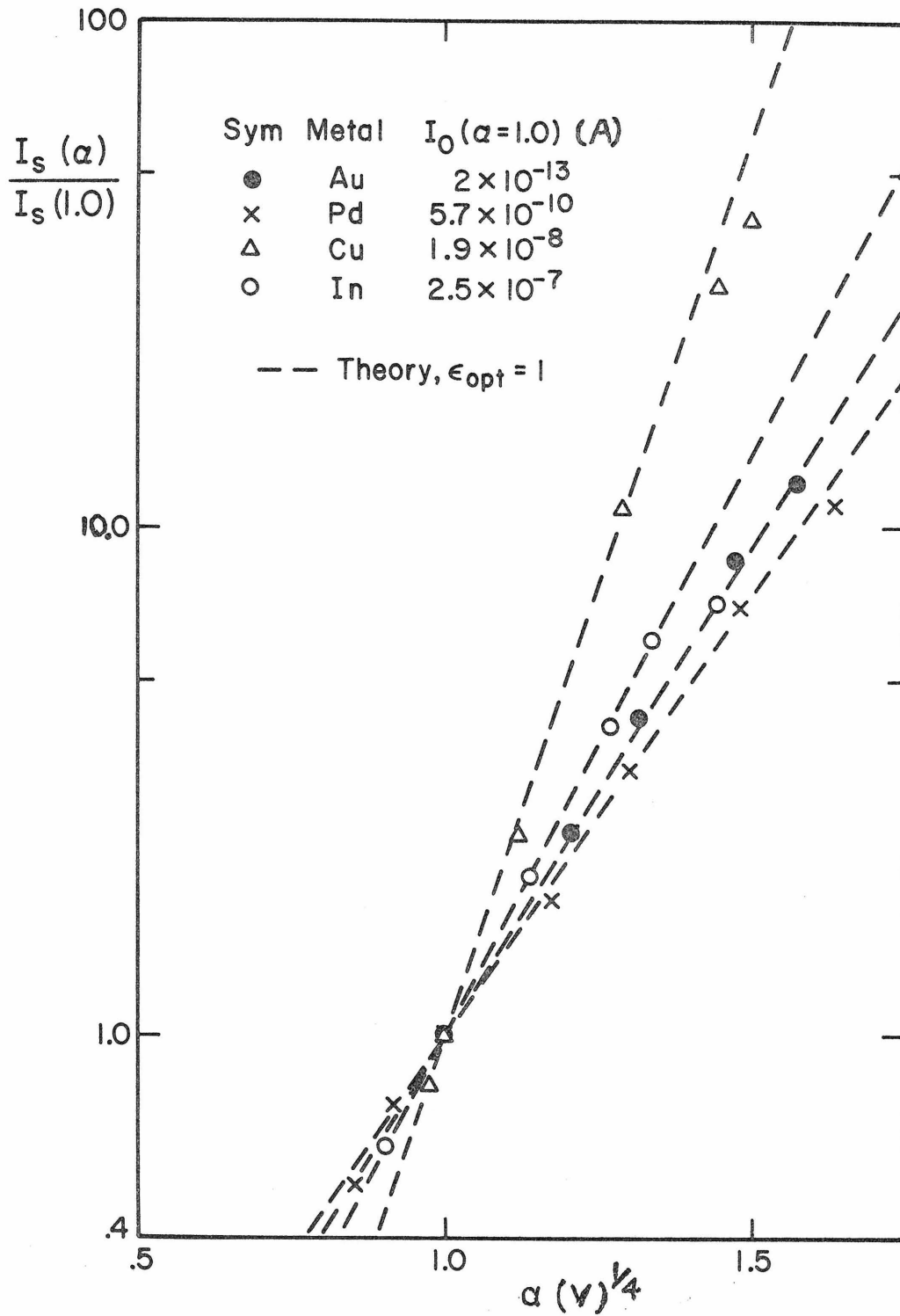the Fermi level less applied voltage and kT/q, is given in Fig. 2.8 for

Fig. 2.8 The logarithm of the normalized reverse current versus alpha for surface barriers on cleaved strontium titanate at 300°K. $\alpha = (\phi_o - \zeta - kT/q - V)^{1/4}$.

gold, palladium, copper, and indium surface barriers. Measurements were made in the dark using a battery and variable resistor as a power supply. The observed currents at α equal to 1 were in the 10^{-4} to 10^{-13} ampere range and were measured with an electrometer and a digital voltmeter.

From the discussion of thermionic theory in Appendix A the log reverse current is expected to vary as the fourth root of the barrier energy less the Fermi level less the applied voltage. Using a room temperature low frequency dielectric permittivity of 330 (Sec. 2.6) and an optical permittivity of unity the dashed lines in Fig. 2.8 were calculated indicating good agreement between experiment and calculation. In conclusion, in both forward and reverse directions the image force correction to the current-voltage curve is consistent with a unity optical dielectric constant.

2.6 Dielectric Investigation

Though used extensively in capacitors as a dielectric, no systematic study of the relative permittivity, ϵ_r, of pure crystalline strontium titanate has been conducted. Values in the literature, over the temperature range from 4.2°K to 300°K, show a considerable variation[36-46]. An investigation was conducted to obtain reliable values of the relative permittivity in order to understand the dielectric properties of this material, determine if it is ferroelectric, and to assist in the interpretation of the surface barrier energies.

The observed relative permittivity of strontium titanate has been attributed to a soft optical mode phonon[51-53]. Soft mode optical phonons are frequently associated with the presence of ferroelectricity[51,54].

In the literature[34,46] there exists evidence both for and against the ferroelectricity of strontium titanate. If strontium titanate is ferroelectric it will possess a Curie temperature, though the converse is not necessarily true[51,56,57]. For ferroelectric material the Curie temperature marks a fundamental change in the dielectric properties. Below the Curie temperature, in the ferroelectric state, high relative permittivity, thermal and electrical hysteresis are common. At the Curie temperature the dielectric relative permittivity often exhibits a discontinuity or a sharp high-valued peak. Above the Curie temperature the material is not ferroelectric, but ε_r frequently exhibits a high value for the relative permittivity. Attempts were made to observe hysteresis, discontinunities in ε_r or a peak value in ε_r but no such evidence of ferroelectricity was observed.

The soft mode phonon responsible for the large dielectric constant has a minimum frequency of $\sim 5 \times 10^{10}$ at $4.2°K$[53]. This is in the infrared spectrum and should not produce a dielectric constant which is a detectable function of the frequency at frequencies less than 10^8 Hz. Strontium titanate is known to have a domain structure at low temperatures as a result of the $65°K$ and $110°K$ phase transitions[29]. Interaction of domains and an applied electric field has produced variation in the dielectric constant of barium titanate at frequencies between 10^6 Hz and 10^8 Hz[58]. To determine if the strontium titanate domain effects are analogous, capacitance measurements were made at frequencies from 10^5 to 5×10^7 Hz.

2.6.1 Measurements

Strontium titanate wafers were used as the dielectric in capacitors. The area to thickness ratio was much greater than unity to minimize fringing capacitance effects. Capacitance bridges were used to measure the capacitance of the sample devices at frequencies between 5 KHz and 50 MHz. For some measurements, of a qualitative nature, at frequencies between 1 MHz and 50 MHz a twin channel oscilloscope and signal generator were used with the scope monitoring the voltage across the test sample and across a resistor in series with the sample. A battery with a variable resistor was used to bias the test samples. Both polarities of test bias were applied to all samples. The temperature of the test sample was adjusted by placing the sample in a twin-walled cryogenic probe. By adjusting the flow of a cold or warm gas through the space between the tube walls the temperature could be varied continuously from 4.2°K to 300°K. The temperature was held constant during each measurement. Capacitance measurements were made at successively decreasing temperatures and then made for successively increasing temperatures. At each temperature the electric field was progressively increased in one direction, then decreased, and then increased again.

Typical capacitance data are presented in Fig. 2.9 as log C as a function of the log T with the applied field strength as a parameter. As the temperature decreases from 300°K to 65°K the capacitance rises smoothly and remains independent of applied field strength. At 65°K the lattice undergoes a transition from tetragonal to orthorhombic[29] and the capacitance becomes dependent upon the field strength. This dependence increases smoothly with decreasing temperature.
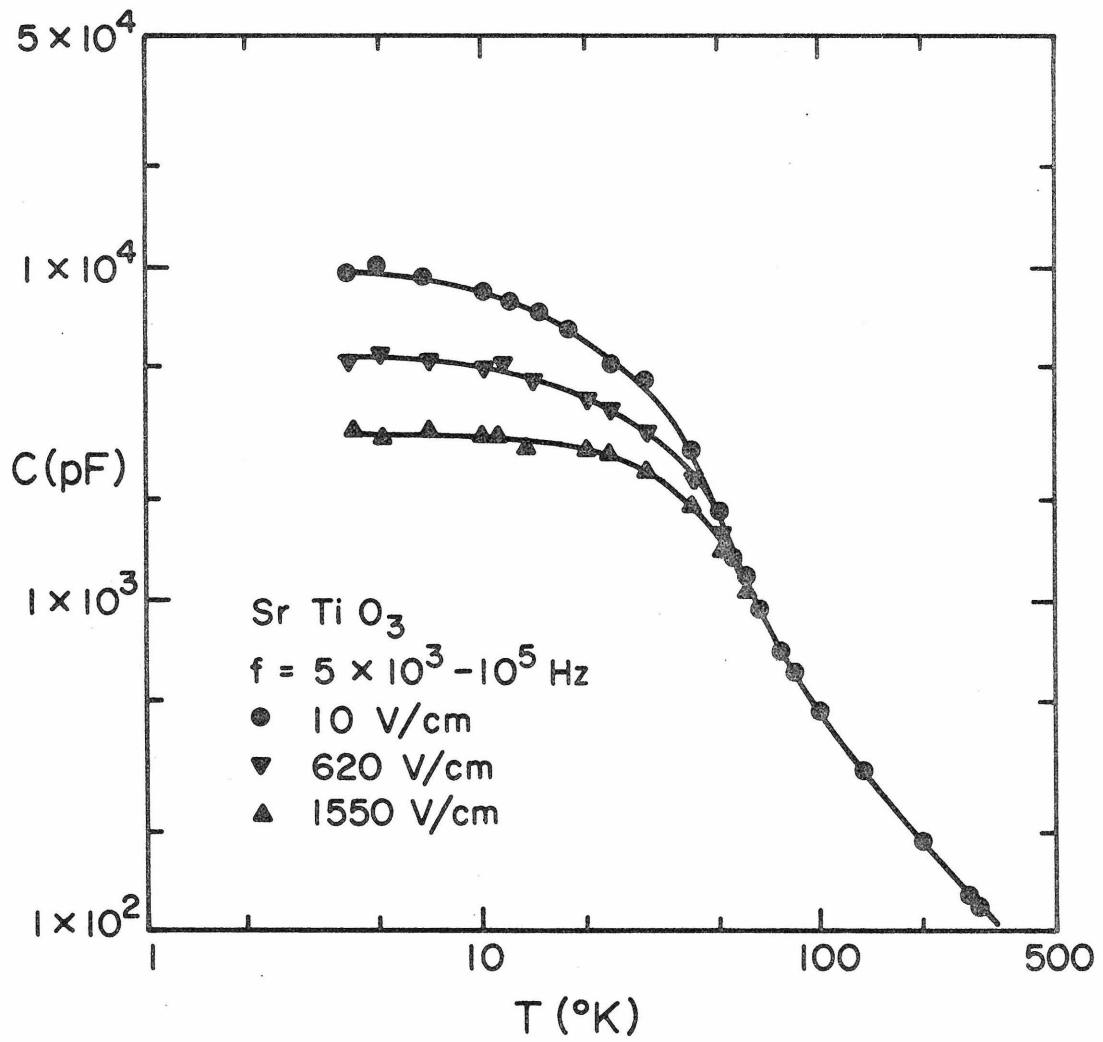
Fig. 2.9 Typical log capacitance as a function of log temperature
with electric field strength as a parameter.

2.6.2 Discussion of the Relative Permittivity

The relative permittivity of strontium titanate can be computed from the parallel plate capacitance values measured using:

$$\varepsilon_r = \frac{W}{\varepsilon_o} \frac{C}{A} = 1 + \frac{1}{\varepsilon_o} \frac{\partial P}{\partial E} \approx \frac{1}{\varepsilon_o} \frac{\partial P}{\partial E} \qquad (2.1)$$

$$\varepsilon_r \gg 1$$

Where: P is the polarization

E is the applied electric field strength

ε_o is the permittivity of free space

A is the area

C is the measured capacitance

W is the capacitor dielectric thickness.

At room and liquid nitrogen temperatures the value of ε_r was determined for frequencies between 5 KHz and 50 MHz with applied DC bias field between −29,900 and + 29,900 V/cm. The values obtained were 330 and 1910 for 300°K and 77°K, respectively, for the (100) oriented crystals. The dielectric constant at these temperatures was found to be electric field and measurement frequency independent. The field independence of ε_r at 300°K indicates that the small capacitance variations considered in Sec. 2.4 for surface barrier devices cannot be the result of changes in the dielectric constant with bias.

The relative permittivity of strontium titanate at measurement frequencies between 5×10^3 and 1×10^5 Hz and at temperatures from 4.2°K to 300°K is given in Table 2.3 for applied electric field strengths

E_k (V/cm) $T(°K)$	10	100	200	620	1080	1550
4.2	26500	24000	21000	14400	10800	8600
10	23200	21700	19000	13500	10300	8400
15	20200	19000	17600	12200	9600	8000
20	17100	16300	14800	11000	9000	7700
30	12000	11500	11000	8700	7800	6600
40	8100	7900	7500	6700	6200	5400
50	4900	4900	4800	4800	4400	4100
60	3200	3200	3150	3150	3100	3100
70	2300	2300	2300	2300	2300	2300
77	1880	1880	1880	1880	1880	1880
100	1280	1280	1280	1280	1280	1280
120	910	910	910	910	910	910
200	550	550	550	550	550	550
280	357	357	357	357	357	357
300	330	330	330	330	330	330

Table 2.3

Relative permittivity, at measurement frequencies of 5×10^3 to 10^5 as a function of temperature and DC field strength

to 1550 V/cm.   Typical values of the relative permittivity are presented

in Fig. 2.10.   The relative permittivity was found to be independent of

the field strength at temperatures in excess of 65°K.   Below this temp-

erature the relative permittivity is dependent on the field.   The rela-

tive permittivity is everywhere a smooth function of the temperature with

no sign of electrical or thermal hysteresis.

The Curie temperature of a material is obtained by observing the

inverse dielectric constant as a function of temperature.   The inverse

dielectric constant, for an ideal ferroelectric material, is given by[51]:

$$\frac{1}{\epsilon_r} = \frac{T-T_c}{A} \qquad (2.2)$$

Where: A is a constant independent of the temperature, T,

T_c is the Currie temperature.

The inverse relative permittivity of strontium titanate is presented as a

function of temperature for a bias of 10 V/cm in Fig. 2.11.   Also

included in this figure are the data taken by Weaver[40] between room and

liquid nitrogen temperatures at the same bias.   The Curie-Weiss law,

depicted as a dashed line is followed from 300°K to 40°K with the

extrapolated intercept, for infinite relative permittivity, the Curie

temperature.   The Curie temperature has been found to be 30°K + 3°K for

strontium titanate.

During these measurements of capacitance the temperature was

repeatedly swept through the Curie temperature (25°K to 45°K) as well as

through the regions of expected phase transition temperature, 10°K, 65°K,

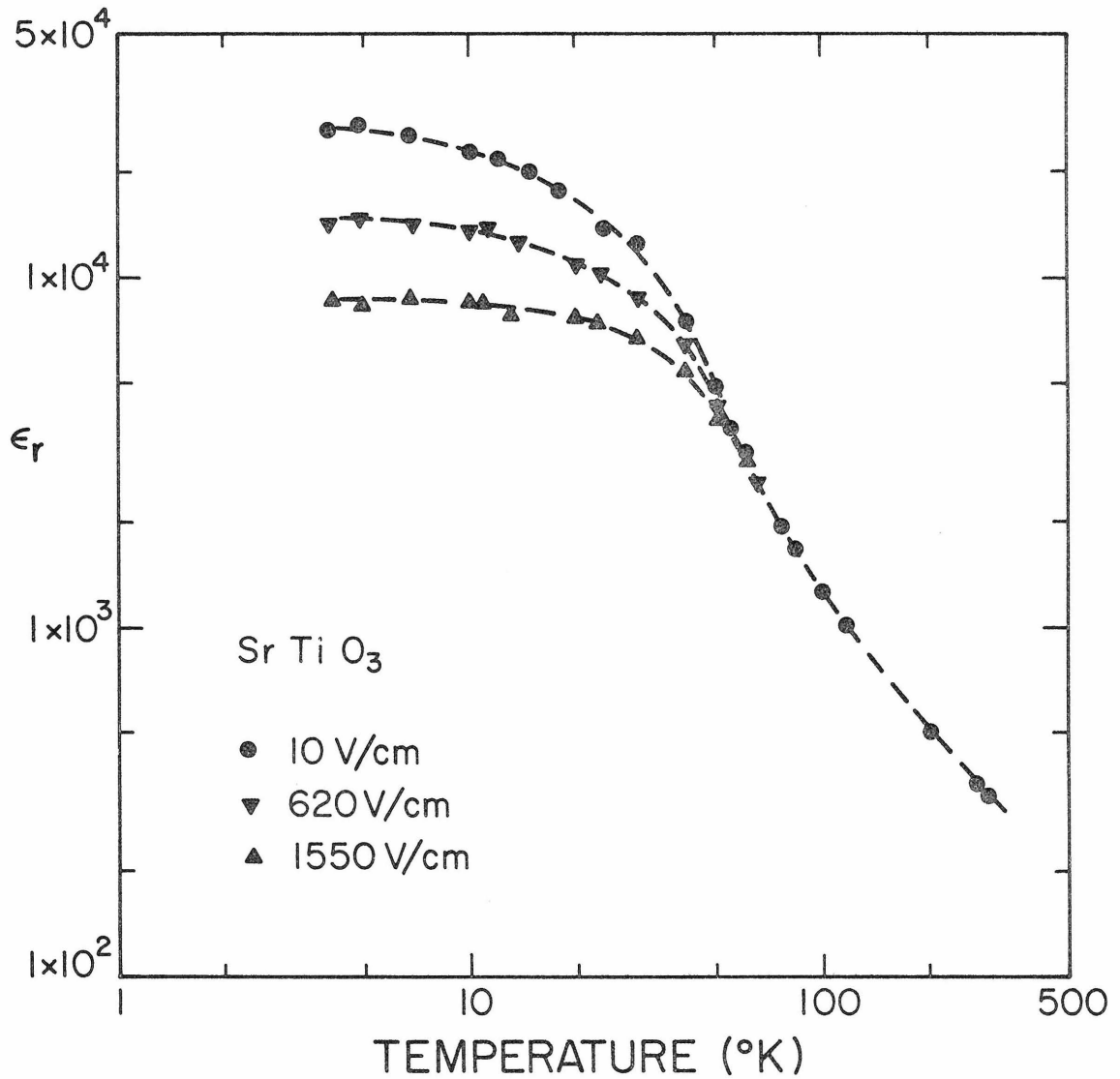and 110°K[29].   No indication of a peak value in the permittivity or of

Fig. 2.10 Log relative permittivity of strontium titanate as a function
of the logarithm of temperature with applied field strength
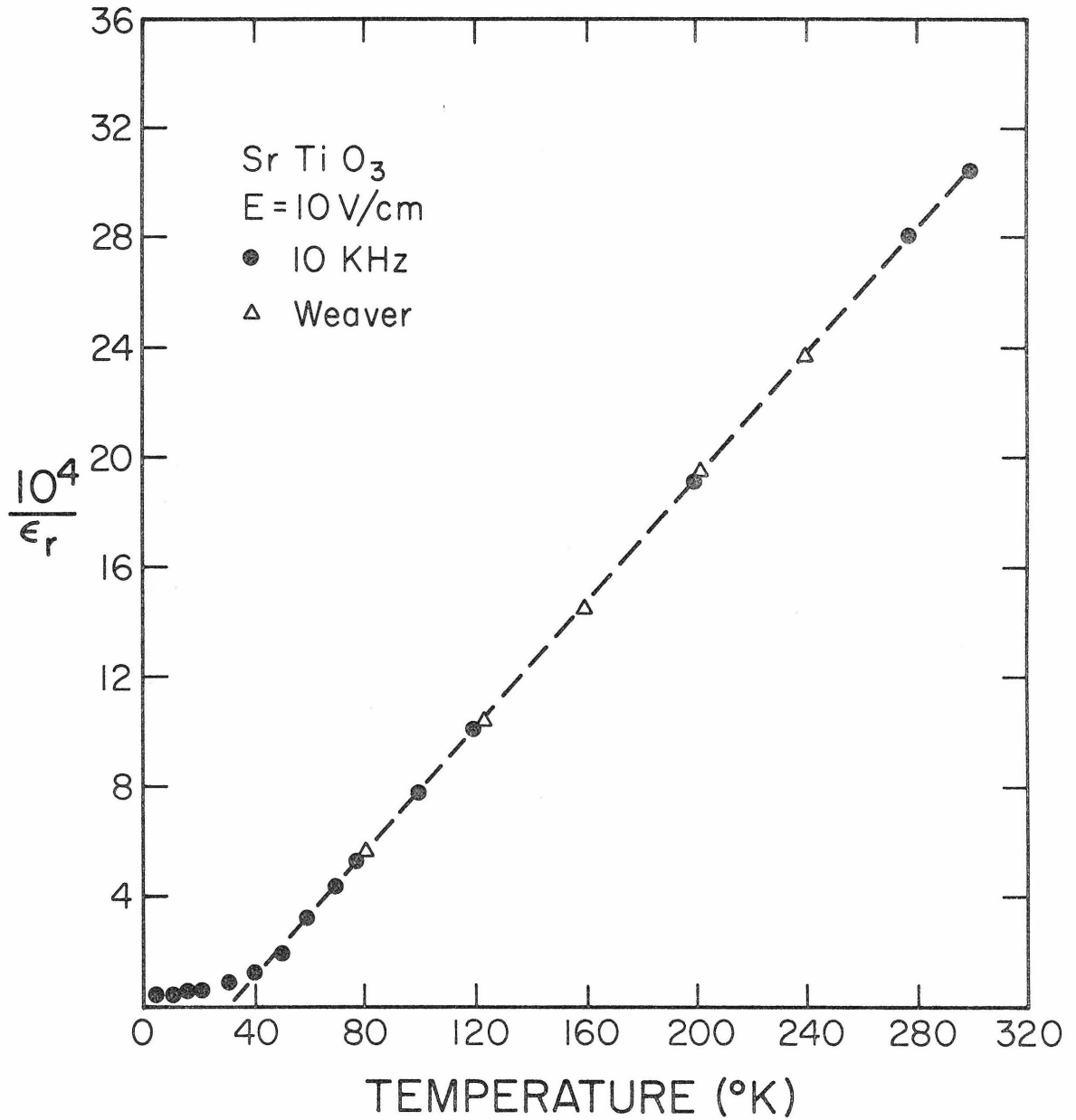as a parameter. Above 65°K each point represents all field
strengths,

Fig. 2.11 Inverse relative permittivity versus temperature for
strontium titanate.

thermal or electric field hysteresis was observed. Even below 65°K, where the relative permittivity is a function of the applied field, there is no evidence of thermal or electrical hysteresis and no peak or discontinuity in the values of the relative permittivity at any temperature. At no point is there evidence of a ferroelectric transition. The transition to a ferroelectric material, if such a transition exists, must be at a temperature below 4.2°K.

An anomalous frequency dependence of the capacitance and, therefore, of the relative permittivity was found in the 10^5 to 10^7 Hz frequency range for temperatures below 65°K. The capacitance was found to vary rapidly with frequency with peak values of the dielectric constant followed by minima occurring in the 10^6 - 3 x 10^7 Hz range. The measured capacitance and its change with frequency and applied bias were non-reproducable and were dependent on the value of the last applied DC field. Such behavior has been observed in barium titanate and attributed to domains.

In order to suppress the domains, a large 23,000 V/cm bias was applied to the sample at room temperature and the sample was cooled to liquid helium temperature through the 110°K and 65°K phase transformations. This created an internal energy situation favoring a single domain structure. The capacitance was independent of frequency from 5 x 10^3 Hz to 5 x 10^7 Hz. The values of dielectric constant determined, at 10^4 Hz, on this sample as a function of field at 4.2°K were slightly less than that observed on samples cooled to 4.2°K from 300°K without electrical bias. The observed behavior with and without the field is that expected

from a multiple-domain sample, with the domains arising from the 65°K tetragonal to orthorhombic transition.

2.7 Structural Energy Relationships

The large temperature dependent dielectric constant of strontium titanate can be understood in terms of the crystal structure and the vibrational freedom available to the system. Other titanates, such as barium titanate, exhibited large dielectric constants and many are ferroelectric. In these systems, it has been shown[51] that the dielectric constant is a result of vibrations of the titanium ion. In strontium titanate the titanium ion is surrounded by 6 oxygen ions at $\sim$2 $\overset{\circ}{A}$[54]. The dielectric constant of strontium titanate can then be considered as arising from a phonon which is the result of titanium atom motion.

The phonon modes in any dielectric material interact with an applied electric field, but only at low frequencies. At optical frequencies the titantium ion cannot follow the applied field. The dielectric constant has been shown to follow[55]:

$$\frac{\varepsilon_r(o)}{\varepsilon_r(\infty)} \; = \; \Pi_i \left(\frac{\omega_{Li}}{\omega_{Ti}} \right)^2 \tag{2.3}$$

Here, the ω_{Li} and ω_{Ti} are longitudinal and transverse (relative to the applied field) optical phonon frequencies, $\varepsilon_r(\infty)$ is the optical frequency relative permittivity and $\varepsilon_r(o)$ the low frequency relative permittivity. This expression, known as the LST relation was examined using values of $\varepsilon_r(o)$ obtained here at 15 temperatures in conjunction with the temperature dependent soft mode phonon frequency at the same temperatures from the literature[53]. The relative permittivity at optical

frequencies and the hard phonon modes are independent of temperature[43,53].

Therefore, it is expected from theory that the product of the square of the soft phonon frequency, ω_{TS}, and the low frequency relative permittivity will be independent of temperature. The product of the square of the measured phonon frequency and the measured low frequency dielectric constant is given by:

$$\omega_{TS}^2 \; \varepsilon_r(o) \;\; = \;\; 3.2 \times 10^{-6} \; cm^{-2} \tag{2.4}$$

The product is independent of temperature as expected from theory and therefore, strontium titanate behaves as would be expected on the basis of the soft mode phonon theory.

The free energy of oscillation of the titanium atom cam be seen to be related to the measured relative permittivity[55,56] by considering the energy stored in an applied electric field and applying the first and second laws of thermodynamics[51]. For a relative permittivity large compared to unity the free energy, F, can be written:

$$\frac{1}{\varepsilon_r} \;\; = \;\; \varepsilon_o \frac{\partial^2 F}{\partial P^2} \;\; = \;\; \varepsilon_o \frac{\partial E}{\partial P} \tag{2.5}$$

Where: P is the polarization.

An empirical description for the relative permittivity of strontium titanate, for temperatures from 4.2°K to 300°K, measurement frequencies of $5 \times 10^3 - 10^5$ Hz and applied electric field strengths at and below an absolute magnitude of 1550 V/cm is given by:

$$\frac{1}{\varepsilon_r} \;\; = \;\; \gamma(T-T_c) + N_1(T) + N_2(T)|E| \tag{2.6}$$

Where: $\gamma(T-T_c)$ describes a Curie-Weiss behavior at all temperatures with

$$T_c = 30°K$$
$$\gamma = 1.122 \times 10^{-5} °K^{-1}.$$

The absolute value sign on the field strength denotes symmetry with direction of applied electric field. Both $N_1(T)$ and $N_2(T)$ are functions of the temperature and vanish identically for temperatures in excess of 65°K, the tetragonal to orthorhombic phase transformation temperature.

Values of N_2, the field strength dependent portion of the inverse dielectric constant, can be determined from ε_r and are presented in Fig. 2.12 as a function of the cube of reduced temperature. Also presented in Fig. 2.12, as a solid line, is the functional dependence of N_2 upon the temperature as given by Eq. (2.7). It can be seen that Eq. (2.7) is an excellent representation of the experimental data.

$$N_2(T) = 5.05 \times 10^{-8} (1-(T/65)^3) \quad T \leq 65°K$$
$$N_s(T) = 0 \quad T \geq 65°K$$

(2.7)

The electric field independent portion of the susceptibility, $N_1(T)+\gamma(T-T_c)$ remains positive throughout the temperature range studied. Values for $N_1(T)$ and $\gamma(T-T_c)$ were determined from the values of ε_r and are presented in Fig. 2.13. The empirically derived dependence of $N_1(T)$ upon T is given by Eq. (2.8) and is also shown as a solid line in Fig. 2.13. Again it can be seen that Eq. (2.8) is an excellent representation of the experimental data.
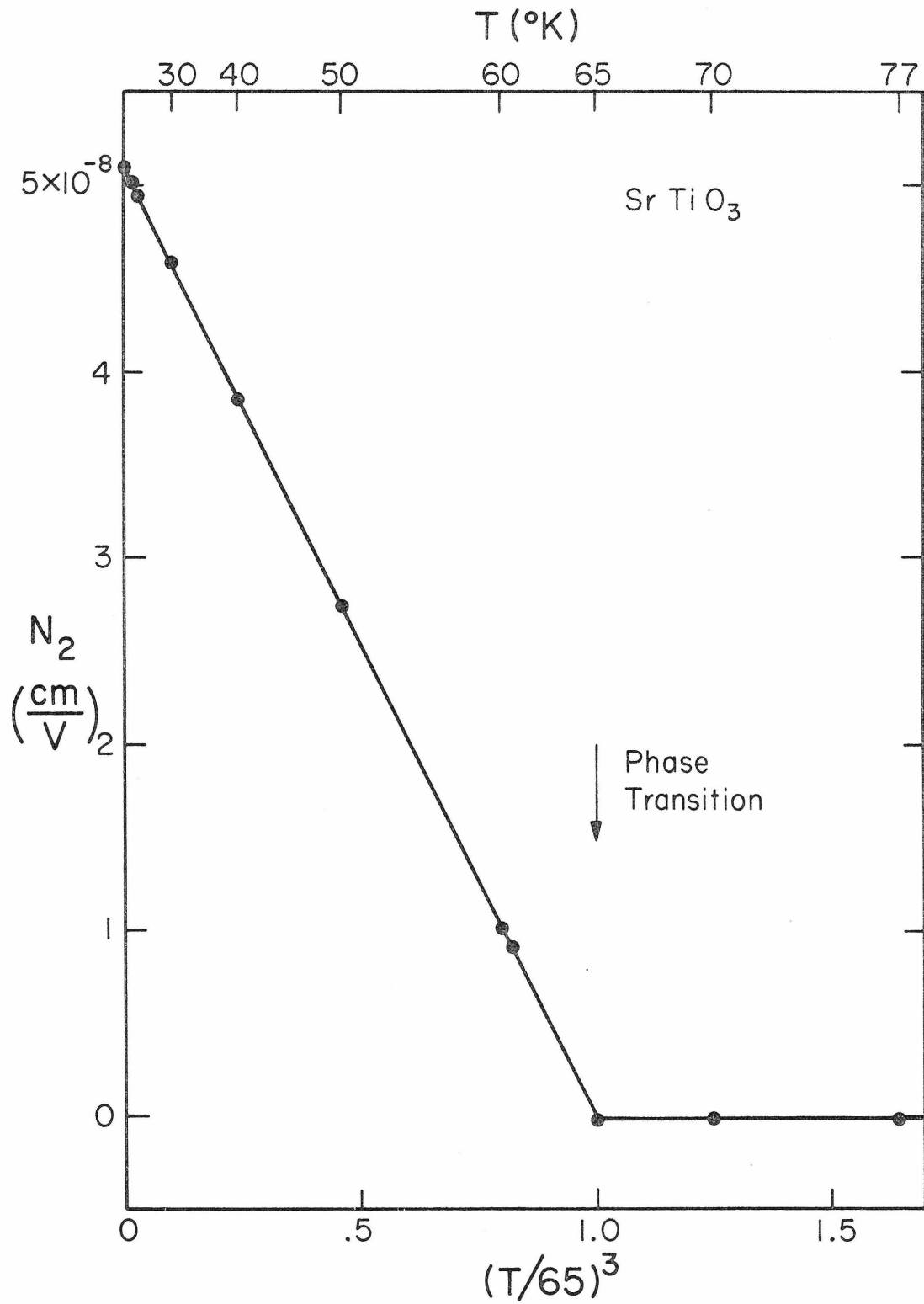
Fig. 2.12 N_2 as a function of the cube root of the reduced temperature.
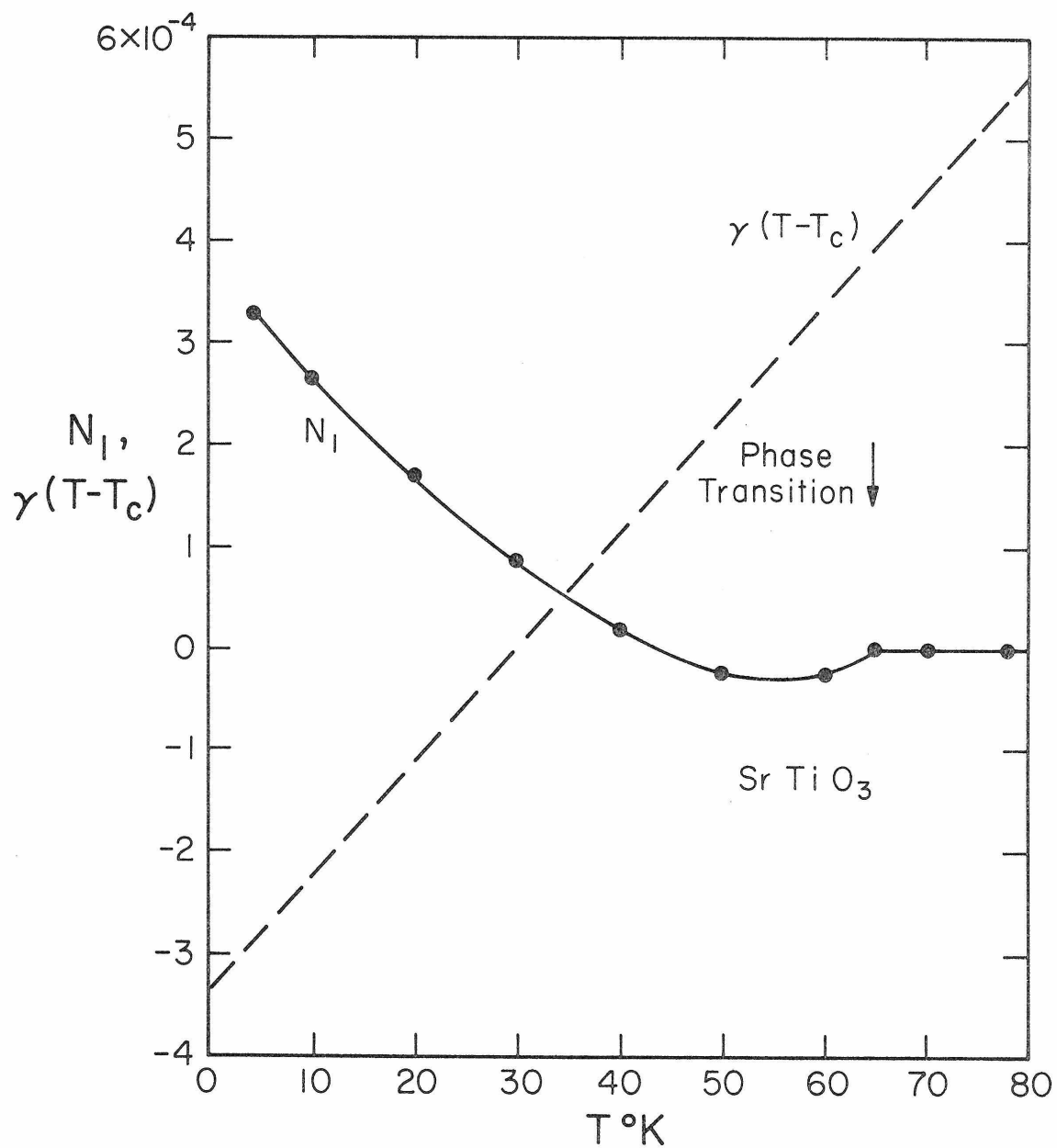
Fig. 2.13 Field strength independent portion of the dielectric constant versus temperature.

$$N_1(T) = 3.73 \times 10^{-4} (1 - \frac{T}{34.5} + \frac{T^2}{7600}) (1 - (\frac{T}{65})^3) \quad T \leq 65°K$$

$$N_1(T) = 0 \qquad\qquad\qquad\qquad\qquad\qquad\qquad\qquad T \geq 65°K$$

$$(2.8)$$

The free energy of the titanium ion can now be determined. The free energy was related to the inverse dielectric constant by a second order differential equation in Eq. (2.5) and an empirical expression for the inverse dielectric constant was presented in Eq. (2.6). By equating these expressions and solving the second order differential equation, an expression for the free energy is:

$$F = g_0 + \frac{g_2 \epsilon_0^2}{N_2^2} \left(e^{\frac{N_2 P}{\epsilon_0}} - 1 - \frac{P N_2}{\epsilon_0} \right) \qquad (2.9)$$

Where: $\epsilon_0 g_2 = \gamma(T - T_c) + N_1(T)$ and the polarization is always positive.
The initial term, g_0, is a constant dependent on the choice of energy reference.

The free energy expression Eq. (2.9) is presented as a function of polarization in Fig. 2.14 with temperature as a parameter. The solid lines in the figure are computed from Eq. (2.9). The data points represent values of polarization and free energy computed from measured values of the dielectric constant (Eq. (2.5, 2.9)). The dashed lines represent the behavior the free energy would have if N_1 and N_2 were zero. This behavior is given by:

$$F = g_0 + \frac{\partial (T - T_c)}{2} P^2 \qquad (2.10)$$

Below 65°K the free energy, for a given polarization, is seen to be less than that above 65°K. For polarization on the order of 10^{-6} Q/cm^2 the free energy departs from the quadratic form and increases more rapidly with polarization. Above 65°K N_1 and N_2 are zero and the expression Eq. (2.10) is an exact description of the free energy as a function of polarization.

The polarization can be considered to be a normalized distance. Then, Fig. 2.14 is a picture of the energy versus distance relationship of the titanium ion. Because the free energy change as a function of polarization is less for a given displacement at low temperatures, the ion moves a greater distance when in a small A C electric field and the relative permittivity is larger at low temperatures. Application of large D C electric fields, large enough to displace the ion to the point at which the energy increases sharply with polarization, will reduce the displacement per unit A C field and causes the observed decrease of ε_r with increasing electric field.

The electric field is related to the polarization by the relative permittivity in Eq. (2.1) and to the free energy by Eq. (2.5). From the expression for free energy, Eq. (2.9):

$$E = \frac{\partial F}{\partial P} = \frac{g_2 \varepsilon_0}{N_2} \left(e^{\frac{N_2 P}{\varepsilon_0}} - 1 \right) \qquad (2.11)$$

For temperatures in excess of 65°K this expression reduces to the Curie-Weiss expression:

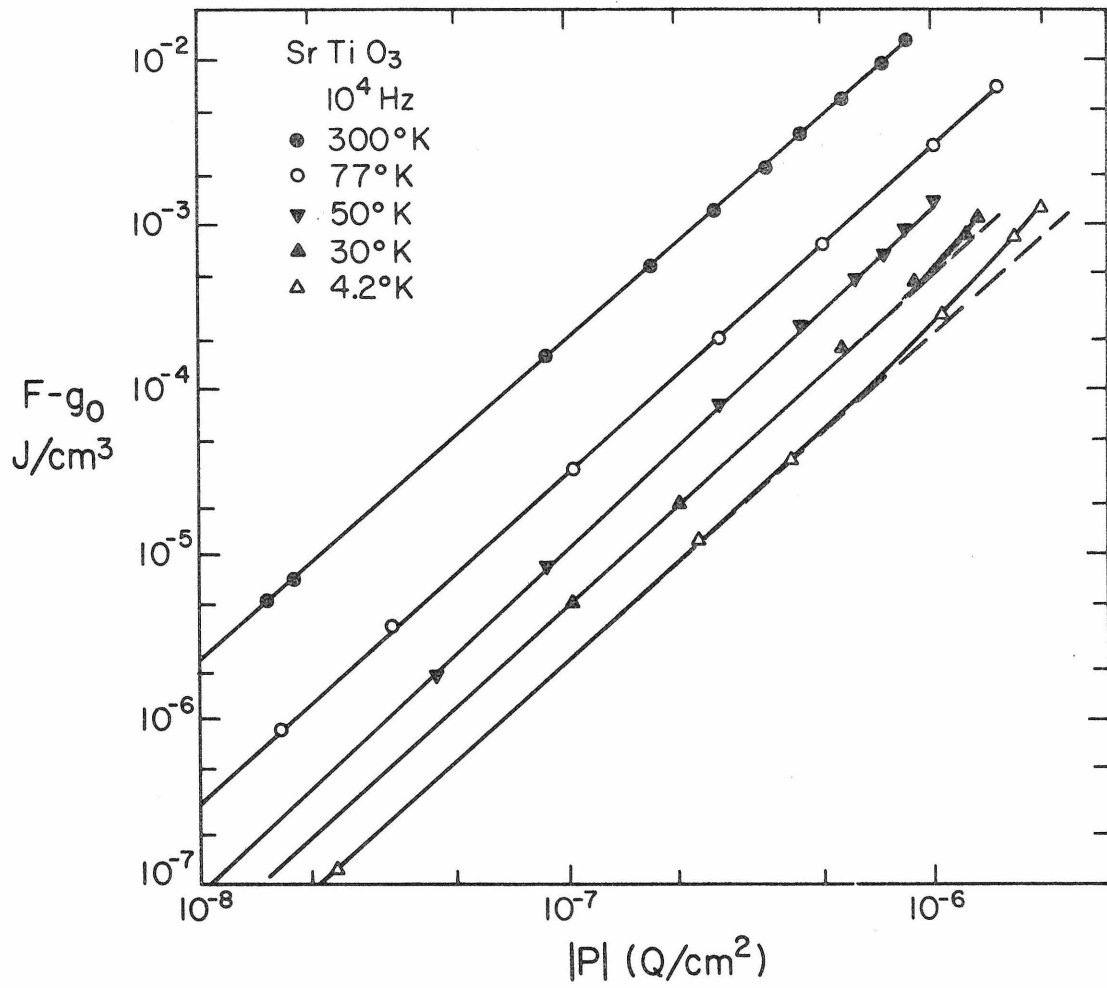$$E = g_2 P = \frac{\gamma(T - T_c)}{\varepsilon_0} P \qquad (2.12)$$

Fig. 2.14 The log of free energy versus the log polarization for strontium titanate with temperature as a parameter.

In Fig. (2.15) the electric field is presented as a function of the polarization with temperature as a parameter. The solid lines in Fig. 2.15 are computed values of polarization using Eq. (2.11). The dashed lines are the Curie-Weiss approximation to the field-polarization relation, Eq. (2.12). The data points represent values of polarization computed from measured values of the dielectric constant. At temperatures of 77°K and 300°K the polarization is a linear function of the electric field. Below 65°K a significant decrease in polarization with applied electric field is observed. This decrease is a result of the sharply increasing free energy of the titanium ion as the ion displacement is increased.

2.8 Strontium Titanate - Conclusion

Surface barrier energy measurements at 300°K were made on both chemically prepared and cleaved strontium titanate crystals. Gold, palladium, copper, and indium Schottky barriers were examined using photo-response, forward current versus voltage characteristics, thermal activation energy, and capacitance variation with voltage techniques. The surface barrier energies for the first three methods are listed in Table 2.2. They show a high degree of consistency and provide the first adequate measure of surface barrier energies on strontium titanate. The chemically prepared surface barrier energies are seen to be slightly lower barrier energies than those obtained on the cleaved surfaces. Such results are consistent with the presence of foreign surface states on the chemically prepared surfaces. The variation of the capacitance with voltage is erratic and the value of capacitance measured is much
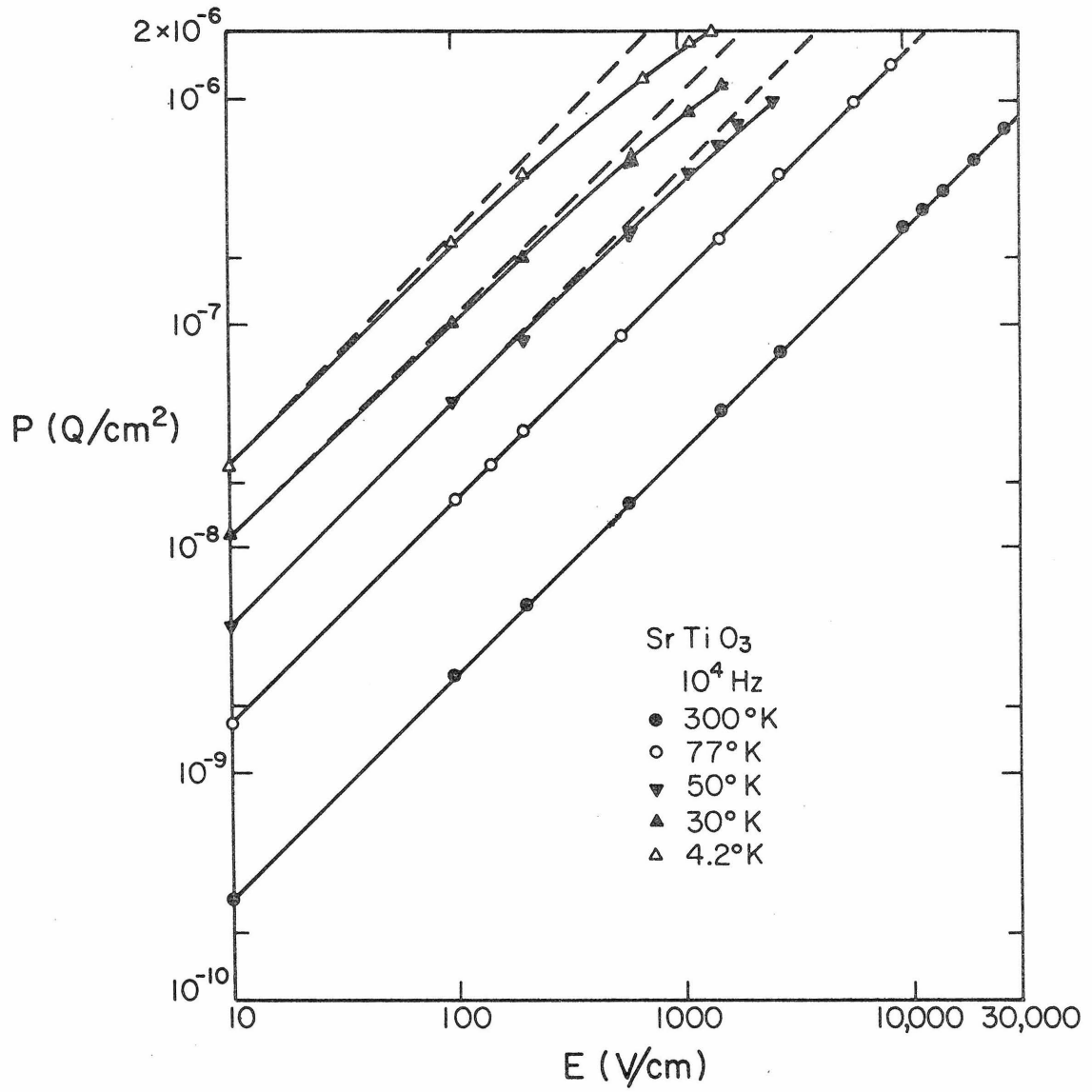
Fig. 2.15 Logarithm of polarization versus the logarithm of the
electric field for strontium titanate with temperature
as a parameter.

less than that predicted by theory. The barrier energies obtained from an extrapolation of the Y_c^2 vs V plot vary widely from barrier to barrier and sometimes are even in excess of the band gap energy. The reasons for this behavior are not understood since in every other way strontium titanate is well behaved. Current voltage characteristics measured on both chemically prepared and cleaved strontium titanate surfaces agree with simple Bethe diode theory as modified by image force lowering using an optical dielectric constant of unity.

Measurements of the relative permittivity at temperatures between 4.2 °K and 300°K as a function of applied bias field strength at low $(5 \times 10^3 - 10^5$ Hz) frequencies were made. Between 65°K and 300°K the relative permittivity increased with decreasing temperature but was electric field independent. Below 65°K, the tetragonal to orthorhombic phase transition temperature, the relative permittivity was electric field dependent. The results obtained for these measurements are in agreement with the titanium-oxygen soft mode phonon theory of temperature sensitive dielectric permittivity and obey the Lyddane-Sachs-Teller relation. Despite a careful search, no evidence of a ferroelectric transition was discovered. A phenomenological description of the free energy of the titanium ion as a function of polarization was empirically derived. The free energy versus polarization characteristic provides insight into the energy versus distance relationship of the titanium ion, responsible for the high dielectric constant of strontium titanate. A non-repeatable variation in observed capacitance was observed in the 10^5 Hz to 5×10^7 Hz frequency range below 65°K. Application of a high (23,000 V/cm) DC

electric field during cooling from room temperature to liquid helium temperature eliminated the anomalous behavior. This finding is consistent with the removal of multiple crystalline domains by application of electrical stress while cooling through the phase transitions at 65°K.

Appendix A

Barrier Energy Determination

Photo-Emission

Given a Schottky barrier with geometry as defined in Fig. 1.2 of Chapter 1 the photon excited current density, J, across the barrier is given by Fowler[17] as:

$$J = q \int_{\phi - h\nu + E_F}^{\infty} v(x) \, N(E) \, P_e(E) \, dE \qquad (A.1)$$

Where q is the electron charge, ϕ is the barrier energy, E_F the Fermi level, x is in the plane of the paper perpendicular to the junction; $v(x)$ is the carrier velocity; and $N(E)dE$ is the electron density of states per unit volume between E and E + dE and $P_e(E)$ is the Fermi probability. Using the Boltzmann approximation to the Fermi function $P_e(E)$ and from $E = \frac{1}{2} (mv^2)$

$$J = \frac{qm^{*3}}{4\pi^3 \hbar^3} \int \frac{v_x \, dv_x \, dv_y \, dv_z}{1 + \exp[\frac{m^*}{2kT} (v_x^2 + v_y^2 + v_z^2) - E_F/kT]} \qquad (A.2)$$

Where m^* is the effective mass, $\hbar$ is Planck's constant over 2π, k is the Boltzmann constant, T is the temperature and the limitations of integration are from:

$$v_x \text{ from } \sqrt{\frac{2}{m^*} (\phi - h\nu + E_F)} \text{ to } \infty$$

$$v_y \text{ from } -\infty \qquad (A.3)$$

$$v_z \text{ from } -\infty \text{ to } \infty$$

Integrating and taking:

$$U = \frac{m^* v_x^2}{2kT} \quad , \quad A_2 = E_F/kT$$

$$J = \frac{9m^* k^2 T^2}{2\pi^2 \hbar^3} \int_{\frac{\phi-hv+E_F}{kT}}^{\infty} \ln\,(1+A_2 1^{-4})\,dU \qquad (A.4)$$

For $hv \approx \phi$, $hv - \phi > 2kT$

$$J \propto (hv-\phi)^2 \qquad (A.5)$$

The barrier energy may be found from the extrapolated zero current intercept of a plot of the square root of the photon generated current versus photon energy.

Thermionic Forward Voltage - Current Characteristic

For thermionic current the diode current is given by Bethe[9] as:

$$J = J_o\,(\exp\,(\frac{qv}{kT}) - 1) \qquad (A.6)$$

$$J_o = A^* \exp\,(\frac{-q\phi}{kT}) \qquad (A.7)$$

$$A^* = \frac{qm^*}{2\pi^2 \hbar^3}\,(kT)^2 \qquad (A.8)$$

The effects of image force lowering, a phenomenon considered in detail in Appendix B, can be included by using in the barrier energy ϕ

$$\phi = \phi_o - \left(\frac{q^3 N_D}{8\pi^2 \epsilon_{opt}^2 \epsilon_r \epsilon_o^3} \right)^{1/4} \quad (\phi_o - \zeta - V - \frac{kT}{q})^{1/4} \qquad (A.9)$$

$$= \phi_o \quad - \Delta\phi$$

where: A^* is known as Richardson's constant[18], ϵ_{opt} is the optical frequency dielectric constant, ϵ_r is the low frequency dielectric constant, ϕ_o is the barrier energy, N_D is carrier impurity density, ζ is the difference in energy between the Fermi level and the conduction band edge and J_o is the reverse saturation current.

$$\zeta = \frac{kT}{q} \quad \ln \frac{N_c}{N_D} \qquad (A.10)$$

where N_c is the conduction band density of states. For voltages such that the exponential term in Eq. A.6 exceeds unity by a factor of ~10 or more:

$$J = A^* \exp \quad \left(- \frac{q}{kT} \quad (\phi_o - \Delta\phi - V) \right) \qquad (A.11)$$

Taking the logarithm to the base e

$$\ln \frac{J}{A^*} = \frac{q\phi_o}{kT} + \frac{q\Delta\phi}{kT} + \frac{qV}{kT} \qquad (A.12)$$

Differentiating where $\frac{\partial \Delta\phi}{\partial V}$, $\frac{\partial \Delta\phi}{\partial \phi_o} \ll 1$

$$\partial \ln \frac{J}{A^*} = \frac{-q\partial\phi_o}{kT (1 + \frac{\partial \Delta\phi}{\partial \phi_o})} + \frac{q \, \partial V}{kT (1 - \frac{\partial \Delta\phi}{\partial V})} \qquad (A.13)$$

Integrating:

$$J = A^* \exp\left(\frac{-q\phi_o}{nkT}\right) \quad \exp \left(\frac{qV}{nkT}\right) \tag{A.14}$$

where:

$$n = 1 + \frac{\partial \Delta\phi}{\partial(\phi_o - \zeta - v)} \tag{A.15}$$

(See also Sze[19] and Henish[20]

From A.13 the surface barrier energy is given by

$$\phi_o = \left. \frac{nkT}{q} \ln \frac{A^*}{J} \right|_{V = 0} \tag{A.16}$$

Thermal Activation Energy

The reverse biased current, or leakage current, for a diode in the thermionic mode including image force lowering is given by:

$$J_R = \frac{A^*}{T^2} \quad T^2 \exp\left(\frac{-\phi_o + \Delta\phi}{kT/q}\right) \tag{A.17}$$

Variation in the barrier temperature while maintaining a fixed reverse bias will produce:

$$\frac{\partial \ln J_R/(A^*/T^2)}{\partial 1/T} = - 2T - \frac{\phi_o + \Delta\phi}{k/q} - \frac{q}{kT} \frac{(\phi_o - \Delta\phi)}{\partial 1/T} \tag{A.18}$$

If ϕ_o and $\Delta\phi$ are temperature independent we have:

$$\phi_o = \phi_A = \frac{-k}{q} \left[\frac{\partial \ln J_R(v)}{\partial 1/T}\right] - \frac{2kT}{q} \tag{A.19}$$

where:

ϕ_A is known as the thermal activation energy

For an ionic crystal it can be shown that[22,23]

$$\frac{\partial \phi}{\partial T} = \frac{\phi_o}{Eg} \frac{\partial E_g}{\partial T} < 0 \qquad (A.20)$$

and over a limited range of temperature

$$\phi = \phi_o + A_1 T, \quad A_1 < 0 \qquad (A.21)$$

For

$$\frac{\partial \Delta \phi}{\partial T} << \frac{\partial \phi}{\partial T}$$

$$\phi_o = \phi_A + \frac{q}{kT} \frac{\phi_o}{E_g} \frac{\partial E_g}{\partial T} \qquad (A.22)$$

From Park[2] the band gap energy for zinc oxide is 3.435. The change in forbidden gap, E_∂, with temperature for zinc oxide has been found to be 8×10^{-4} eV/°K [24] near 300°K. For zinc oxide A_1 has values close to -1.5×10^{-4} eV°K.

For strontium titanate Gandy[30] has determined the band gap energy to be 3.15eV. The change in forbidden gap, E_g, with temperature has been determined to be -8.5×10^{-4} eV/°K near 300°K.[49] For Pd on strontium titanate then the value of A_1 is $\sim 2.8 \times 10^{-4}$ eV/°K.

Capacitance - Voltage

Consider Eq. (B.4) in Appendix B. Squaring this equation and inverting we have where C is the capacitance:

$$\phi_o - \zeta - V - \frac{kT}{q} = \frac{q\varepsilon_r\varepsilon_o}{2} N_D \frac{1}{(C/A)^2} \qquad (A.23)$$

The barrier energy can be found from the intercept on the voltage axis of a plot of $1/C^2$ vs V, a knowledge of ζ, the Fermi level, and the temperature.

Appendix B

Capacitance - Voltage Relationships

The metal side of a metal-semiconductor junction has a very high density of fixed charges in comparison to even a degenerately doped semiconductor. Applying a reverse bias to a Schottky barrier results in a depletion region which to first order may be considered as extending solely into the semiconductor. Applying Gauss's law and assuming a constant relative permittivity:

$$\nabla^2 \psi = -\rho/\varepsilon = -\frac{qN_D}{\varepsilon_r \varepsilon_o} \tag{B.1}$$

Where we take our conventions from Fig. 1.2, q is the electronic charge, N_D is the density of fixed charged donor atoms, ε_r is the low frequency dielectric constant and ε_o is the permittivity of a vacuum. We take as our reference point the barrier and set $\psi(0) = 0$. The other boundary condition which we need is $E(X_D) = 0$, where X_D is the maximum value of the depletion layer width and E is the electric field. Integrating:

$$\psi(X) = \frac{qN_D}{\varepsilon_r \varepsilon_o} \ (XX_D - X^2/2) \tag{B.2}$$

The applied voltage is -V volts. Then:

$$\phi_o - \zeta - V - \frac{kT}{q} = \psi(X_D) = \frac{qN_D}{\varepsilon_r \varepsilon_o} \ \frac{X_D^2}{2} \tag{B.3}$$

The differential capacitance of a Schottky barrier is:

$$\frac{C}{A} = \frac{\partial Q}{\partial V} = \sqrt{\frac{\varepsilon_r \varepsilon_o q}{2}} \sqrt{\frac{N_D}{\phi_o - \zeta - V - \frac{kT}{q}}} \tag{B.4}$$

Squaring (B.4) and taking the derivative with respect to V we obtain the carrier concentration:

$$N_D = \frac{2}{q\varepsilon_r\varepsilon_o} \left(1/ \frac{\partial(A/C)^2}{\partial V} \right) \qquad (B.5)$$

An electron approaching the energy barrier from the right (in the semi-conductor) sees an image of itself. The force on the electron is[59]:

$$F = \frac{q^2}{4\pi\varepsilon_{opt}\varepsilon_o(2X)^2} = -q\,\nabla(\Delta\phi) \qquad (B.6)$$

Where ε_{opt} is the optical frequency dielectric constant. Integrating (B.6) we obtain a potential:

$$\Delta\phi = \frac{q}{16\pi\varepsilon_{opt}\varepsilon_o X} \qquad (B.7)$$

The net potential in the depletion field region is given by:

$$\phi(X) = \frac{qN_D}{\varepsilon_r\varepsilon_o} \left(XX_D - \frac{X^2}{2} \right) + \frac{q}{16\pi\varepsilon_{opt}\varepsilon_o X} \qquad (B.8)$$

At some distance, X_C, the image force potential results in an electric field strong enough to counter-balance the electric field produced by the built in and applied bias. For distances smaller than X_C the image force field is then dominant, while for $X > X_C$ the bias and built in electric fields are the principal fields. At $X = X_C$ the fields counter-act and:

$$0 = \frac{qN_D}{\varepsilon_r\varepsilon_o} (X_D - X_C) - \frac{q}{16\pi\varepsilon_{opt}\varepsilon_o X_C^2} \qquad (B.9)$$

From Eq. B.3:

$$X_C = \left(\frac{q\, \varepsilon_r}{\varepsilon_{opt}^2 \varepsilon_o 2(16^2) \pi^2 N_D} \right)^{1/4} \qquad \left(\frac{1}{(\phi_o - \zeta - V - \frac{kT}{q})^{1/4}} \right) \qquad (B.10)$$

Substituting Eq. (B.10) into (B.8) and considering only first order terms in X_C we find $\phi(X_C)$ which is the image force lowering potential as:

$$\Delta\phi = \phi(X_C) = \left(\frac{q^3 N_D (\phi_o - \zeta - V - \frac{kT}{q})}{8\pi^2 \varepsilon_{opt}^2 \varepsilon_r \varepsilon_o^3} \right)^{1/4} \qquad (B.11)$$

Appendix C
Tunneling and Thermionic Field Emission Theories

In heavily doped semiconductors the Fermi level can be several kT/q into the conduction band. The current at low temperatures is a result of tunneling by electrons through the surface barrier.[10-14] The current is determined by the probability of transmission through the barrier, the available supply of electrons and the available places for the electrons on the opposite side of the barrier.[11] The electron supply function in the semiconductor is given by $N(E)dE\ P(E)$ where $N(E)dE$ is the density of states at energy E and $P(E)$ is the Fermi probability. In the metal a number of states $N(E)dE\ (1-P(E))$ is available to receive electrons. The tunneling probability is given by[27]

$$\text{Prob} = \exp\left(-2 \int_{x_1}^{x_2} \frac{P}{\hbar}\ dx\right) \tag{C.1}$$

where the limits of integration are given by the classical turning points of the barrier and P is the carrier momentum.

For material as degenerate as the zinc oxide used, the electron supply involved in the tunneling arises from an energy region centered on the Fermi energy level and $1/S_m$ in width where S_m is defined in equation C.3.[14] This case was treated in detail by Millea et al[12]. The current density, for a bias in excess of kT/q is given by:[12]

$$J = J_m \exp\ (-\Delta S_m)\ \approx\ J_m \exp\ S_m(V-\phi) \tag{C.2}$$

$$S_m = \frac{2}{\hbar}\left(\frac{\varepsilon_o \varepsilon_r}{N_d}\ m^*\right)^{1/2} \tag{C.3}$$

$$\Delta = (\phi_B - V)^{1/2} (\phi_B + .6\zeta - V)^{1/2}$$

$$- .6\zeta \left(\ln \frac{(\phi_B - V)^{1/2} + (\phi_B + .6\zeta - V)^{1/2}}{(0.6\zeta)^{1/2}} \right) \approx (\phi_B - V) \qquad \text{(C.4)}$$

$$J_m = \frac{A^*}{(C_1 kT)^2} \ \frac{\pi C_1 kT}{\sin \pi C_1 kT} \qquad \text{(C.5)}$$

$$C_1 = \frac{S_m}{2} \ln \left(\frac{4(\phi_B - V)}{.6\zeta} \right) \qquad \text{(C.6)}$$

where: $\hbar$ is Plank's constant divided by 2π

m^* is the effective mass

ε_o is the permittivity of free space

ε_r is the dielectric constant at low frequencies

N_d is the carrier concentration

k is Boltzmann's constant

T is the temperature

A^* is Richardson's constant (see Appendix A)

ϕ_B is the barrier energy

V is the applied voltage

ζ is the Fermi level relative to the conduction band

The second order correction to the tunneling probability derived by Landau and Lifshitz[27] and considered in chapter one consists of setting:

$$\text{Prob} = \frac{1}{P} \ \exp \left(-2 \int_{x_1}^{x_2} \frac{P}{\hbar} \ dx \right) \qquad \text{(C.7)}$$

The effect is to reduce the tunneling current magnitudes.

An upper temperature limit for pure field emission has been shown to be[10,25]:

$$\left(C_1 + \sqrt{\frac{S_m}{2\zeta}} \right)^{-1} > kT \tag{C.8}$$

As the temperature increases electrons are excited to elevated energy states in the semiconductor conduction band. At these elevated states, lower in energy than the barrier energy, the electrons then tunnel through the barrier, much reduced in thickness from the barrier thickness at the Fermi level. This mode of current conduction is a combination of thermionic and tunneling modes and has been developed theoretically by Padovani and Stratton.[10] They have found the current to be given by:

$$J = J_o \exp SV \tag{C.9}$$

Where:

$$J_o = A^* \left\{ \sqrt{\frac{1}{S_m \pi}} \; (\phi_B - V + \zeta)^{1/2} \Big/ \; kT \cosh \left(\frac{1}{S_m kT} \right) \right\} \delta \tag{C.10}$$

$$\delta = \exp \left(\frac{\zeta}{kT} - S(\phi_B + \zeta) \right) \tag{C.11}$$

$$S = S_m \tanh \left(\frac{1}{S_m kT} \right) \tag{C.12}$$

The thermionic-field emission expressions Eqs. C.9-C.12 have been shown valid for temperatures satisfying[10]

$$kT > \left(\frac{2}{S_m} \right) \left\{ \ln \left[\frac{4(\phi_B - V)}{\zeta} \right]^{-1} \right\} \tag{C.13}$$

An upper temperature limit is imposed by the onset of current via thermal emission over the surface barriers. Padovani and Stratton have

found this to be:[10]

$$\frac{\text{Cosh}^2 \left(\frac{1}{S_m kT}\right)}{\text{Sinh}^3 \left(\frac{1}{S_m kT}\right)} < 2(\phi_B + \zeta - V) \frac{S_m}{3} \tag{C.14}$$

REFERENCES

1. H. E. Brown, Zinc Oxide Rediscovered, New Jersey Zinc Co., New York 1957.

2. Y. S. Park, et al., Phys. Rev. 143, 512 (1966).

3. H. Rupprecht, J. Phys. Chem. Solids 6, 144 (1958).

4. G. Bogner, J. Phys. Chem. Solids 19, 235 (1961).

5. R. J. Collins and D. A. Kleinman, J. Phys. Chem. Solids 11, 190 (1959).

6. R. C. Dietz, et al., J. Appl. Phys. 32, 2282 (1961).

7. C. A. Mead, Phys. Lett. 18, 218 (1965).

8. J. F. Dewald, Bell System Technical J. 39, 615 (1960).

9. H. A. Bethe, MIT Radiation Laboratory Report: 43/12 (1942).

10. F. A. Padovani and R. Stratton, Solid State Elec. 9, 695 (1966).

11. J. W. Conley and G. D. Mahan, Phys. Rev. 161, 681 (1967).

12. M. Millea, M. McColl, and C. A. Mead, Phys. Rev. 177, 1164 (1969).

13. G. H. Parker and C. A. Mead, Appl. Phys. Lett. 14, 21 (1969).

14. G. H. Parker, Thesis California Institute of Technology (1969).

15. J. L. Moll, Physics of Semiconductors, Chap. 5 McGraw-Hill (1964).

16. R. A. Smith, Semiconductors, Chap. 4,5 Cambridge Press, Cambridge, (1959).

17. R. H. Fowler, Phys. Rev. 38, 45 (1931).

18. C. R. Crowell, Solid State Elec. 8, 395 (1965).

19. S. M. Sze, et al., J. Appl. Phys. 35, 2534 (1964).

20. H. K. Henish, Rectifying Semiconductor Contacts, Clarendon, Oxford (1957).

21. American Institute of Physics Handbook (McGraw-Hill, New York, (1957).

22. R. H. Bube, Private Communication (1967).

23. W. Shockley, Electrons and Holes in Semiconductors, 264-270, 335, 520-531, D. Van Nostrand, Princeton, New Jersey (1950).

24. H. Watanube and M. Wada, Jap. J. Appl. Phys. $\underline{3}$, 617 (1964).

25. E. L. Murphy and R. H. Good, Jr., Phys. Rev. $\underline{102}$, 1464 (1956).

26. R. C. Neville and C. A. Mead, J. of Appl. Phys. $\underline{41}$, 3795 (1970).

27. L. D. Landau and E. M. Lifshitz , Quantum Mechanics, 170-185, Addison-Wesley (1958).

28. M. D. Beals, National Lead Co., Private Communication

29. F. W. Lytle, J. Appl. Phys. $\underline{35}$, 2212-5 (1964).

30. H. W. Gandy, Phys. Rev. $\underline{113}$, 795 (1959).

31. W. S. Baer, Phys. Rev. $\underline{144}$, 734 (1966).

32. H. P. R. Frederiske et al., Phys. Rev. $\underline{147}$, 503 (1966).

33. H. P. R. Frederiske et al., Phys. Rev. $\underline{134}$, A442 (1964).

34. H. P. R. Frederiske et al., Phys. Rev. $\underline{161}$, 822 (1967).

35. O. N. Tufte, P. W. Chapman, Phys. Rev. $\underline{155}$, 799 (1967).

36. A. J. Linz, Phys. Rev. $\underline{91}$, 753 (1953).

37. W. Low and E. L. Offenbacher, Sol. State Phys. $\underline{17}$, 167 (1965).

38. Von E. Hegenbarth, Physica Status Solidi $\underline{2}$, 1544 (1962).

39. T. Mitsui and W. B. Westphal, Phys. Rev. $\underline{124}$, 1354 (1961).

40. H. E. Weaver, Phys. Chem. Sol. $\underline{11}$, 274 (1959).

41. G. Rupprecht, Bull. Am. Phys. Soc. $\underline{6}$, 12 (1961).

42. Von H. Itscher and Von H. Gränicher, Helvestica Physica Acta $\underline{37}$, 624 (1964).

43. R. A. Cowley, Phys. Rev. Lett. 9, 159 (1962).

44. G. Rupprecht and R. O. Bell, Phys. Rev. 135A, A748 (1964).

45. Von H. Gränicher, Helvestica Physica Acta 29, 210 (1956).

46. J. F. Youngblood, Phys. Rev. 98, 1201 (1955).

47. J. E. Carnes, A. M. Goodman, J. of Appl. Phys. 38, 3091 (1967).

48. A. M. Goodman, J. Appl. Phys. 34, 329 (1963).

49. R. S. Krogstad, et al., Bull. Am. Phys. Soc. 8, 470A (1963).

50. A. Levin, et al., J. of Opt. Soc. of Am. 737 (1953).

51. C. Kittel, Introduction to Solid State Physics, 3rd Edition, Chap. 13 (1966) John Wiley and Sons.

52. R. A. Cowley, Phys. Rev. B 134, A981 (1964).

53. J. M. Worlock and P. A. Fleury, Phys. Rev. Lett. 19, 1176 (1967).

54. R. O. Bell. and G. Rupprecht, Phys. Rev. 129, 10 (1965).

55. R. H. Lyddane, et al., Phys. Rev. 59, 673 (1941).

56. W. F. Devonshire, Advan. Phys. 3, 85 (1954).

57. W. Cochran, Advan. Phys. 9, 387 (1960).

58. B. Matthews and A. Von Hippel, Phys. Rev. 73 1378 (1948).

59. S. M. Sze, Physics of Semiconductor Devices, 364-367 Wiley-Interscience (1969).